ITUPublications
Recommendations

International Telecommunication Union
Radiocommunication Sector

Recommendation ITU-R M.1851-2

(12/2023)

M Series: Mobile, radiodetermination, amateur and related satellite services

Mathematical models for radiodetermination radar and aeronautical mobile systems antenna patterns for use in interference analyses

Foreword

The role of the Radiocommunication Sector is to ensure the rational, equitable, efficient and economical use of the radio-frequency spectrum by all radiocommunication services, including satellite services, and carry out studies without limit of frequency range on the basis of which Recommendations are adopted.

The regulatory and policy functions of the Radiocommunication Sector are performed by World and Regional Radiocommunication Conferences and Radiocommunication Assemblies supported by Study Groups.

Policy on Intellectual Property Right (IPR)

ITU-R policy on IPR is described in the Common Patent Policy for ITU-T/ITU-R/ISO/IEC referenced in Resolution ITU-R 1. Forms to be used for the submission of patent statements and licensing declarations by patent holders are available from http://www.itu.int/ITU-R/go/patents/en where the Guidelines for Implementation of the Common Patent Policy for ITU-T/ITU-R/ISO/IEC and the ITU-R patent information database can also be found.

Series of ITU-R Recommendations

(Also available online at https://www.itu.int/publ/R-REC/en)

Series	Title
BO	Satellite delivery
BR	Recording for production, archival and play-out; film for television
BS	Broadcasting service (sound)
BT	Broadcasting service (television)
F	Fixed service
M	**Mobile, radiodetermination, amateur and related satellite services**
P	Radiowave propagation
RA	Radio astronomy
RS	Remote sensing systems
S	Fixed-satellite service
SA	Space applications and meteorology
SF	Frequency sharing and coordination between fixed-satellite and fixed service systems
SM	Spectrum management
SNG	Satellite news gathering
TF	Time signals and frequency standards emissions
V	Vocabulary and related subjects

Note: *This ITU-R Recommendation was approved in English under the procedure detailed in Resolution ITU-R 1.*

Electronic Publication
Geneva, 2024

RECOMMENDATION ITU-R M.1851-2

Mathematical models for radiodetermination radar and aeronautical mobile systems antenna patterns for use in interference analyses

(2009-2018-2023)

Scope

This Recommendation describes mathematical models for radiodetermination radar and aeronautical mobile systems antenna patterns to be used for single-entry and aggregate interference analysis. Dependent on the antenna 3 dB beamwidth and first peak side-lobe level, the proper set of equations for both azimuth and elevation patterns may be selected. Both peak, for single interferer, and average patterns, for multiple interferers, are defined.

Keywords

Antenna patterns, current distribution, illumination field, peak and average mask pattern equations

Abbreviations/Glossary

3-D Three dimensional

ADP Antenna directivity pattern

CSC^2 Cosecant squared

SLL Sidelobe level

Related ITU-R Recommendations

Recommendation ITU-R F.699 – Reference radiation patterns for fixed wireless system antennas for use in coordination studies and interference assessment in the frequency range from 100 MHz to 86 GHz

Recommendation ITU-R F.1245 – Mathematical model of average and related radiation patterns for point-to-point fixed wireless system antennas for use in interference assessment in the frequency range from 1 GHz to 86 GHz

Recommendation ITU-R M.1638 – Characteristics of and protection criteria for sharing studies for radiolocation (except ground based meteorological radars) and aeronautical radionavigation radars operating in the frequency bands between 5 250 and 5 850 MHz

Recommendation ITU-R M.1652 – Dynamic frequency selection in wireless access systems including radio local area networks for the purpose of protecting the radiodetermination service in the 5 GHz band

Recommendation ITU-R M.1849 – Technical and operational aspects of ground-based meteorological radars

The ITU Radiocommunication Assembly,

considering

that a mathematical model is required for generalized patterns of antennas for interference analyses when no specific pattern is available for the radiodetermination radar systems and aeronautical mobile,

recognizing

that these mathematical models may not be applicable for all radiodetermination and aeronautical mobile systems, e.g. for some aeronautical mobile telemetry antenna patterns,

recommends

1 that, if measured antenna patterns and/or pattern equations applicable to a radiodetermination radar or aeronautical mobile systems are available in other ITU-R Recommendations or Reports, then those should be used in interference analysis;

2 that, in the absence of information concerning the antenna patterns of the radiodetermination radar or aeronautical mobile system antenna involved, one of the mathematical reference antenna models described in Annex 1 should be used for interference analysis;

3 that, for phased array antennas, if information related to their physical design is available (geometry, number of elements, element spacing, single element radiation pattern and gain), then the patterns for phased array antenna models of Annex 1 should be used;

4 that, for phased array antennas, if information related to their physical design is not available, then antenna patterns for rectangular aperture antenna or linear line source antennas as given in Annex1 should be used in interference analysis;

5 that, when available, measured antenna patterns of antennas which are representative of radiodetermination radar system or aeronautical mobile system antenna involved should be preferred to conduct interference analyses.

Annex 1

Mathematical models for radiodetermination radar and aeronautical mobile systems antenna patterns for use in interference analyses

TABLE OF CONTENTS

1 Introduction

A generalized mathematical model for radiodetermination radar and aeronautical mobile systems antenna patterns are required when these patterns are not defined in ITU-R Recommendations applicable to the radiodetermination radar and aeronautical mobile systems under analysis. Generalized antenna pattern models could be used in analyses involving single and multiple interferer entries, such as that from other radar and communication systems.

This Annex describes proposed antenna patterns to be used. Given knowledge about beamwidth and the first peak side-lobe level, the proper set of equations for both azimuth and elevation patterns may be selected.

The result of typical antenna parameter ranges from ITU-R Recommendations are recorded in Table 1.

TABLE 1

Typical radiodetermination radar antenna parameter limits

Antenna parameter	Units	Description	Minimum value	Maximum value
Transmit and receive frequencies	MHz		420	33 400
Antenna polarization type		Horizontal, vertical, circular		
Antenna type		Yagi element array, parabolic reflector, phased array		
Beam type – most common		Fan, pencil, cosecant squared		
Transmit and receive gain	dBi		25.6	54
Elevation beamwidth (–3 dB)	degrees	Pencil beam	0.25	5.75
		Cosecant squared (CSC^2) (equations (22), (23) and Tables 7, 8)	3.6 (θ_3) 20 (θ_{Max})	3.6 (θ_3) 44 (θ_{Max})
Azimuth beamwidth (−3 dB)	degrees	Pencil beam	0.4	5.75
Elevation scan angle limit	degrees		−60	+90
Azimuth scan angle limit	degrees		30 sector	360
First side-lobe level below main lobe peak	dB		−35	−15.6

Table 1 was used to guide the development of the antenna types and patterns proposed.

2 Mathematical formulae

2.1 Rectangular aperture antenna

2.1.1 Background

If the information about the shape of the current distribution or illumination field on the antenna aperture is accessible, then a more accurate model of the antenna pattern can be used.

To simplify the analysis, the antenna current distribution is considered as a function of either the elevation or azimuth coordinates. The directivity pattern, $F(\mu)$, of a given distribution is found from the finite Fourier transform as:

$$F(\mu) = \frac{1}{2}\int_{-1}^{+1} f(x) \cdot e^{j\mu x} dx \quad (1)$$

where:

$f(x)$: relative shape of field distribution, see Tables 2 and 4 and Fig. 1

μ: provided in the Table below = $\pi\left(\frac{l}{\lambda}\right)\sin(\alpha)$

l: overall length of aperture

λ: wavelength

ω: beam elevation or azimuth pointing (scan) angle relative to aperture normal

θ: point of interest direction angle relative to aperture normal

α: point of interest direction angle relative to pointing angle direction ($\alpha = \theta - \omega$)

x: normalized distance along aperture $-1 \leq x \leq 1$

j: complex number notation.

FIGURE 1

Antenna polar diagram mask

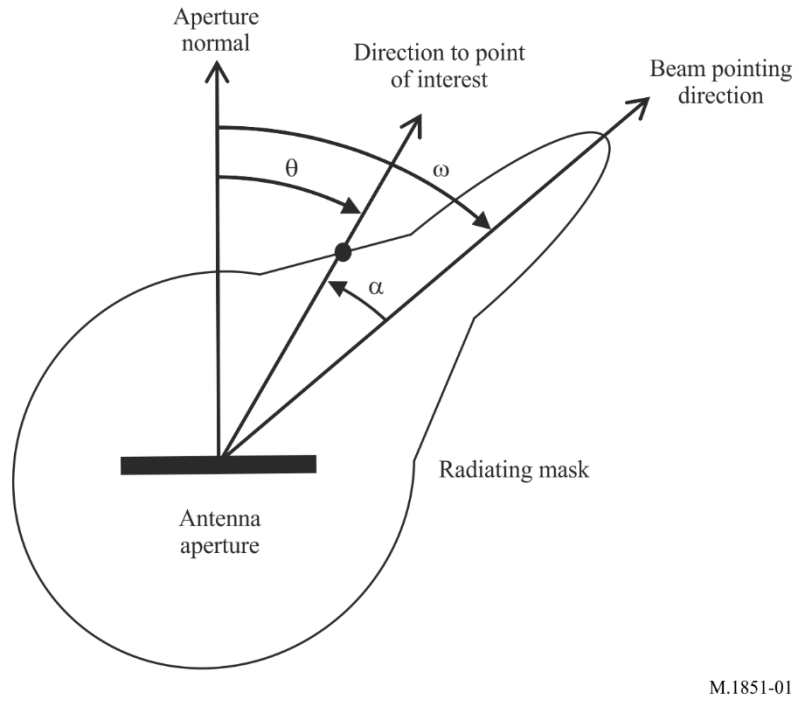

The proposed theoretical antenna patterns for antennas having uniform phase field distribution are provided in Tables 2 and 4.

The parameters and formulae for determining antenna directivity patterns (ADP) are presented in Tables 2 and 4 (and thereafter in the related Tables and Figures) taking into account that field amplitude at the edge of the antenna aperture generally is not equal to zero.

Peak or average masks are recommended for sharing and compatibility studies with radar and aeronautical mobile systems with single or multiple interferers respectively. The mask departs at break point issued from theoretical pattern and decreases over sidelobes down to a floor mask to represent antenna far side lobes and back lobes.

If real radar antenna patterns are available, then those should be digitized and used.

2.1.2 Theoretical antenna equations

Equations of normalised directivity patterns and associated parameters are given in Tables 2 and 3 for different cosine field distribution on the antenna aperture taking into account the level of a pedestal C. Pedestal is a level on the edges of the antenna when the amplitude distribution is normalized. As ω scan angle is denoted. θ_3 is the 3-dB antenna half-power beamwidth (degrees). *SLL* denotes the first sidelobe level below the main beam, in dB. The ranges of sidelobe levels for each amplitude distributions (n = 0, 1 or 2) are shown in the column ‘Range of maximum side-lobe level below normalized main lobe peak (dB)’ of Table 2 for model using pedestal. The normalized directivity patterns and associated parameters for the case without pedestal are given in Table 4.

The difference between these two models is that the first one (Tables 2 and 3) can give any sidelobe level in the range from −13.2 dB to −40 dB, the second model gives discrete values of sidelobe levels −13.2 dB, −23 dB, −32 dB, −40 dB and −47 dB. Also the second model gives much steeper descending envelope of the sidelobes comparing with the first model.

TABLE 2

Theoretical antenna directivity parameters for rectangular aperture antenna

Relative shape of field distribution $f(x)$ with pedestal C where $-1 \le x \le 1$	**Directivity pattern $F(\mu)$ (μ in radians)**	**Coefficient K (°)**	**θ_3 half power beam-width (degrees)**	**μ (in radians) as a function of θ_3 (in degrees)**	**Range of the first side-lobe level below main lobe peak (dB)**	**Equation No.**
Uniform	$\frac{\sin(\mu)}{\mu}$	50.8	$K\left(\frac{\lambda}{l}\right)$	$\frac{\pi . K . \sin(\theta - \omega)}{\theta_3}$	−13.2	(2)
$C + (1 - C)\cos\left(\frac{\pi x}{2}\right)$ (C from equation (5))	$\frac{C\frac{\sin\mu}{\mu} + (1-C)\frac{2}{\pi}\frac{\cos\mu}{1-\left(\frac{2\mu}{\pi}\right)^2}}{C + (1-C)\frac{2}{\pi}}$	Equation (6)	$K\left(\frac{\lambda}{l}\right)$	$\frac{\pi . K . \sin(\theta - \omega)}{\theta_3}$	−22.7 to −13.2	(3)
$C + (1 - C)\cos^2\left(\frac{\pi x}{2}\right)$ (C from equation (7))	$\frac{C\frac{\sin\mu}{\mu} + \frac{(1-C)}{2\mu}\frac{\sin\mu}{1-\left(\frac{\mu}{\pi}\right)^2}}{C + \frac{(1-C)}{2}}$	Equation (8)	$K\left(\frac{\lambda}{l}\right)$	$\frac{\pi . K . \sin(\theta - \omega)}{\theta_3}$	−40 to −22.7	(4)

TABLE 3

Table for selection of antenna parameters for rectangular aperture antenna (cosine taper)

Cosine distribution raised to power n	Range of maximum side-lobe level below normalized main lobe peak (dB)	Pedestal C	Bandwidth factor K (°)
0	−13.2	-	50.8
1	−22.7 to −13.2	$C = 0.0007(SLL + 22.7)^3 - 0.006(SLL + 22.7)^2 + 0.09(SLL + 22.7) + 0.1$ (5)	$K = -0.0117(SLL + 22.7)^3 + 0.217(SLL + 22.7)^2 - 2.46(SLL + 22.7) + 64.2$ (6)
2	−40 … −22.7	$C = 0.0056(SLL + 40)^3 - 0.04(SLL + 40)^2 + 1.1(SLL + 40) + 9.9)/100$ (7)	$K = -0.0013(SLL + 40)^3 + 0.018(SLL + 40)^2 - 0.79(SLL + 40) + 73$ (8)

TABLE 4

Theoretical antenna directivity parameters for rectangular aperture antenna or linear line source without pedestal

Relative shape of field distribution $f(x)$ with pedestal C where $-1 \le x \le 1$	directivity pattern $F(\mu)$ (μ in radians)	θ_3 half power beam-width (degrees)	μ (in radians) as a function of θ_3 (in degrees)	Range of the first side-lobe level below main lobe peak (dB)	Equation No.
Uniform	$\frac{\sin(\mu)}{\mu}$	$50.8\left(\frac{\lambda}{l}\right)$	$\frac{\pi \times 50.8 \times \sin(\theta - \omega)}{\theta_3}$	−13.2	(9)
$\cos\left(\frac{\pi x}{2}\right)$	$\frac{\pi}{2}\left[\frac{\cos(\mu)}{\left(\frac{\pi}{2}\right)^2 - \mu^2}\right]$	$68.8\left(\frac{\lambda}{l}\right)$	$\frac{\pi \times 68.8 \times \sin(\theta - \omega)}{\theta_3}$	−23	(10)
$\cos^2\left(\frac{\pi x}{2}\right)$	$\frac{\pi^2}{2.\mu}\left[\frac{\sin(\mu)}{(\pi^2 - \mu^2)}\right]$	$83.2\left(\frac{\lambda}{l}\right)$	$\frac{\pi \times 83.2 \times \sin(\theta - \omega)}{\theta_3}$	−32	(11)
$\cos^3(\pi * x/2)$	$\frac{3\pi\cos(\mu)}{8}\left[\frac{1}{\left(\frac{\pi}{2}\right)^2 - \mu^2} - \frac{1}{\left(\frac{3\pi}{2}\right)^2 - \mu^2}\right]$	$95\left(\frac{\lambda}{l}\right)$	$\frac{\pi \times 95 \times \sin(\theta - \omega)}{\theta_3}$	−40	(12)
$\cos^4(\pi * x/2)$	$\frac{3\pi^4 \sin(\mu)}{2\mu(\mu^2 - \pi^2)(\mu^2 - 4\pi^2)}$	$106\left(\frac{\lambda}{l}\right)$	$\frac{\pi \times 106 \times \sin(\theta - \omega)}{\theta_3}$	−47	(13)

The three-dimensional (3-D) pattern may be obtained in the following way, in linear units:

$$G_{3D} = G_1(\theta_1) \times G_2(\theta_2) \quad (14)$$

or, in dB:

$$G_{3D,dB} = G_{1,dB}(\theta_1) + G_{2,dB}(\theta_2) \quad (15)$$

where G_{3D}, G_1, G_2 are normalized, G_1 and G_2 are antenna radiation patterns in E and H planes, θ_1 and θ_2 are elevation angles in these planes.

The relative shapes of the different cosine field distribution functions *f*(*x*) with pedestal, as defined in Table 2, and without pedestal, as defined in Table 4, are plotted schematically in Figs 2 and 3, respectively.

FIGURE 2

Aperture distributions with pedestal

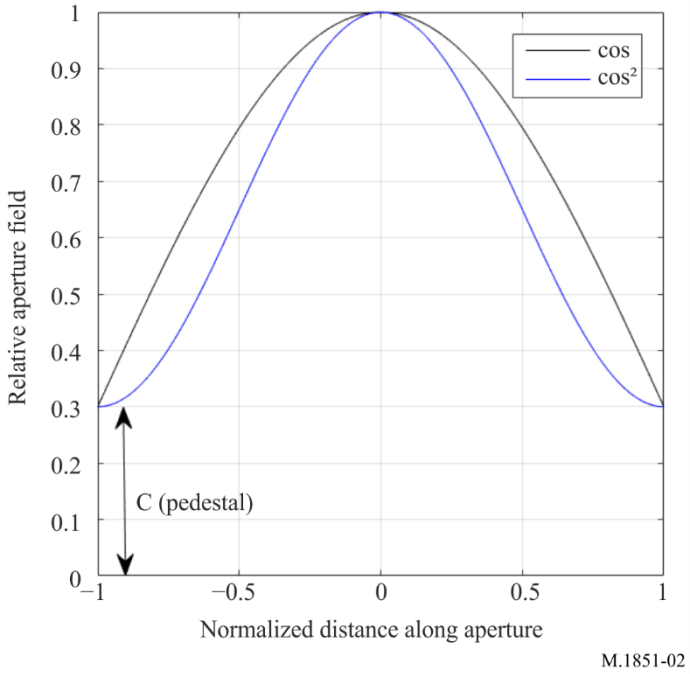

FIGURE 3

Aperture distributions without pedestal

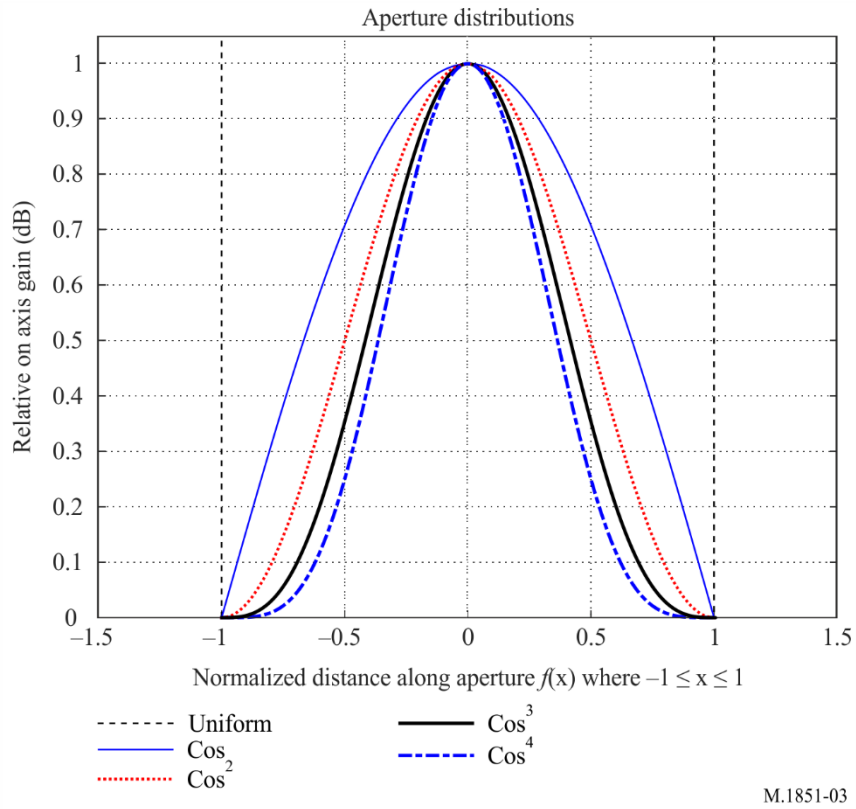

Given that the half power beamwidth, θ_3, is provided, the value of μ can be redefined as a function of the half-power antenna beamwidth. This is done by replacing the quantity $\left(\frac{l}{\lambda}\right)$ in $\mu = \pi\left(\frac{l}{\lambda}\right)\sin(\theta)$ by a constant (beamwidth factor) that depends on the relative shape of the field distribution; divided by the half-power beamwidth, θ_3, as shown in Table 2. Approximations for beamwidth factor are given in Tables 2 and 4; these values can be derived by setting the equation for $F(\mu)$ equal to −3 dB, and solving for the angle θ.

Figure 4 shows various rectangular aperture antenna patterns for uniform, cosine (COS), cosine-squared (COS^2) field distribution functions with pedestal. Figure 5 shows various rectangular aperture antenna patterns for uniform, cosine (COS), cosine-squared (COS^2) and cosine-cubed (COS^3) and cosine-to-the-fourth power (COS^4) field distribution functions without pedestal. As the patterns are mathematically symmetric, they have been partially traced on the diagram. For comparison, all patterns are set to a same 3 dB beamwidth of 6.0 degrees, meaning different ratios for λ/l.

FIGURE 4

Antenna pattern comparison for various rectangular aperture distributions with pedestal, 3 dB beamwidth is 6.0 degrees (pattern is symmetric)

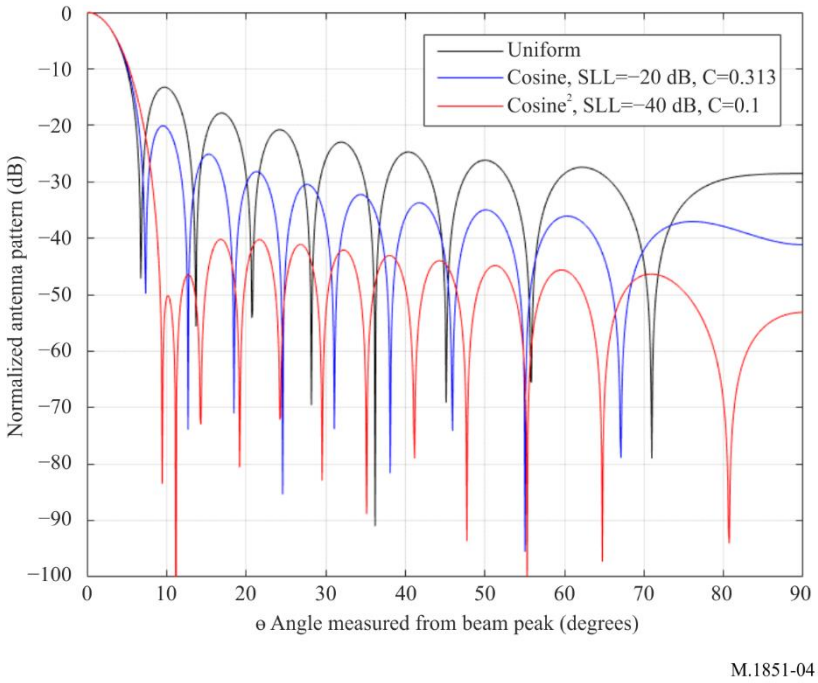

M.1851-04

FIGURE 5

Antenna pattern comparison for various rectangular aperture distributions without pedestal, 3 dB beamwidth is 6.0 degrees (pattern is symmetric)

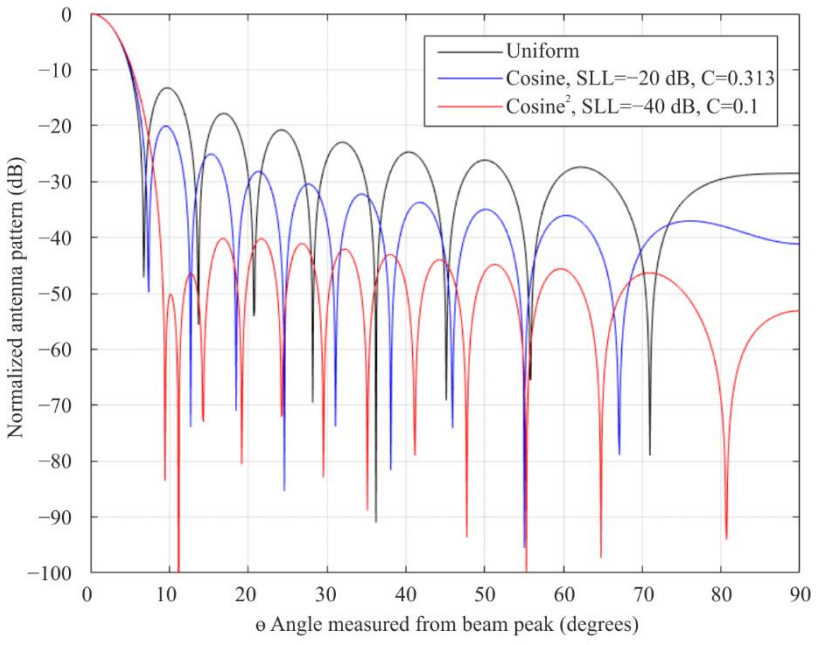

M.1851-05

2.1.3 Procedure for mask determination

Using Figs 4 and 5 above, the mask equations are derived by using a curve fit to the antenna peak side-lobe levels. It has been found, by comparing the integral of the theoretical and the proposed mask

patterns, that the difference between the peak and average power in one principal plane cut is approximately 4 dB. The following definitions apply:

– convert equations (2) to (13) into dB using $20 \times \log_{10}(|\text{Normalized Pattern}|)$;

– normalize the antenna pattern gains for method without pedestal from Table 4. Uniform field distribution does not require normalization, for cosine one subtract −3.92 dB, for cosine-squared one subtract −6.02 dB and for cosine-cubed one subtract −7.44 dB, and for cosine-to-the-fourth power one subtract −8.52 dB (see Table 6); method from Table 2 does not require normalization;

– to plot the mask, use the theoretical directivity pattern from Table 2 for models with pedestal and Table 4 for models without pedestal, as shown in the previous two steps, up to the break point for either the peak or average antenna pattern, as required. After the break point, apply the mask pattern as indicated in Table 5 for models with pedestal and Table 6 for models without pedestal;

– the peak pattern mask is the antenna pattern that rides over the side-lobe peaks. It is used for a single-entry interferer;

– the average pattern mask is the antenna pattern that approximates the integral value of the theoretical pattern. It is used for aggregated multiple interferers;

– the peak pattern mask break point is the point in pattern magnitude (dB) below the maximum gain where the pattern shape departs from the theoretical pattern into the peak mask pattern, as shown in Fig. 6;

– the average pattern mask break point is the point in pattern magnitude (dB) below the maximum gain where the pattern shape departs from the theoretical pattern into the average mask pattern, as shown in Fig. 6;

– θ_3 is the 3 dB antenna beamwidth (degrees);

– θ is the angle in either the elevation (vertical) or azimuth (horizontal) principal plane cuts (degrees);

– the average mask is the peak mask minus 4 dB. Note that the break points of the peak pattern are different from the average patterns;

– the three-dimensional (3-D) pattern may be obtained as $G_{3D} = G_1(\theta_1) + G_2(\theta_2)$, where G_{3D}, G_1, G_2 are normalized and in decibels, G_1 and G_2 are antenna radiation patterns in E and H panes, θ_1 and θ_2 are angles in these planes.

Tables 5 and 6 show the equations to be used in the calculations.

TABLE 5

Equation (16): Peak and average normalised theoretical mask pattern equations for cosine taper with pedestal

Field distribution	Mask equation beyond pattern break point where mask departs from theoretical pattern (dB)	A	B	Mask floor level (dB)
Uniform	$-A \ln \frac{B\lvert\theta\rvert}{\theta_3}$	8.584	2.876	−30
COS		$-0.000473(\text{SLL}+13.2)^5 - 0.008667(\text{SLL}+13.2)^4 - 0.0581(\text{SLL}+13.2)^3 - 0.1455(\text{SLL}+13.2)^2 - 0.1342(\text{SLL}+13.2) + 8.2489$	if $SLL \geq -22.7$ and $SLL \leq -18$: $0.03911\ \text{SLL}^3 + 2.1706\ \text{SLL}^2 + 39.803\ \text{SLL} + 246.52$ if $SLL > -18$ and $SLL < -13.2$: $-0.461\ \text{SLL} - 3.058$	−50
COS^2		$0.000119\ \text{SLL}^3 + 0.00869\ \text{SLL}^2 + 0.2488\ \text{SLL} + 10.37$	$\exp(-0.00027\ \text{SLL}^3 - 0.02255\ \text{SLL}^2 - 0.751\ \text{SLL} - 6.6)$	−60

TABLE 6

Peak and average theoretical mask pattern equations

Field distribution	Normalisation	Mask equation beyond pattern break point where mask departs from theoretical pattern (dB)	Peak pattern break point where mask departs from theoretical pattern (dB)	Average pattern break point where mask departs from theoretical pattern (dB)	Constant added to the peak pattern to convert it to average mask (dB)	Mask floor level (dB)	Equation No.
Uniform	0	$-8.584 \cdot \ln\left(2.876 \cdot \frac{\lvert\theta\rvert}{\theta_3}\right)$	−5.75	−12.16	−3.72	−30	(17)
COS	−3.92	$-17.51 \cdot \ln\left(2.33 \cdot \frac{\lvert\theta\rvert}{\theta_3}\right)$	−14.4	−20.6	−4.32	−50	(18)
COS^2	−6.02	$-26.882 \cdot \ln\left(1.962 \cdot \frac{\lvert\theta\rvert}{\theta_3}\right)$	−22.3	−29.0	−4.6	−60	(19)

TABLE 6 (*end*)

Field distribution	Normalisation	Mask equation beyond pattern break point where mask departs from theoretical pattern (dB)	Peak pattern break point where mask departs from theoretical pattern (dB)	Average pattern break point where mask departs from theoretical pattern (dB)	Constant added to the peak pattern to convert it to average mask (dB)	Mask floor level (dB)	Equation No.
COS^3	−7.44	$-35.84 \cdot \ln\left(1.756 \cdot \frac{\lvert\theta\rvert}{\theta_3}\right)$	−31.5	−37.6	−4.2	−70	(20)
COS^4	−8.52	$-45.88 \cdot \ln\left(1.56 \cdot \frac{\lvert\theta\rvert}{\theta_3}\right)$	−39.4	−42.5	−2.61	−80	(21)

The function ln() is the natural logarithm function. An example of the break point is shown in Fig 6.

FIGURE 6

Break point example

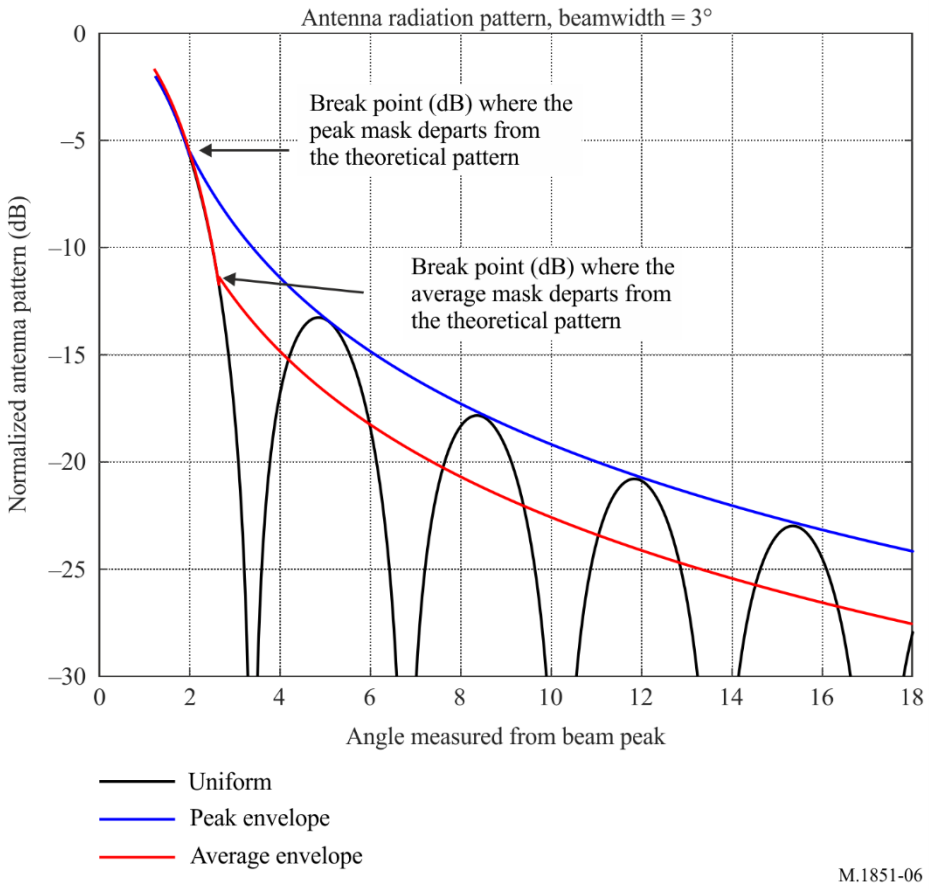

2.2 Antenna with a cosecant-squared elevation pattern

The cosecant-squared pattern (CSC^2) is a special shape which provides to the radar receiver a nearly constant strength of echoes' returns independently of the horizontal range, for aircrafts flying at a constant altitude. Figure 7 shows a typical diagram of range detection performance (km) of radars.

The cosecant-squared normalized power directivity pattern, in dB, is defined piecewise, as follows for ground radars:

$$G_{Ground}(\theta) = \begin{cases} G_{unif}(\theta) \text{ if } \theta \in [\theta_{Null}; \theta_{Start}] \\ G_{csc^2}(\theta) \text{ if } \theta \in [\theta_{Start}; \theta_{End}] \\ G_0 \text{ otherwise} \end{cases} \quad (22)$$

For airborne radars, the cosecant-squared normalized power directivity pattern is given as:

$$G_{Airborne}(\theta) = \begin{cases} G_{unif}(\theta) \text{ if } \theta \in [\theta_{Start}; \theta_{Null}] \\ G_{csc^2}(\theta) \text{ if } \theta \in [\theta_{End}; \theta_{Start}] \\ G_0 \text{ otherwise} \end{cases} \quad (23)$$

where:

$G_{unif}(\theta)$: the normalized power directivity pattern associated with the uniform field pattern (defined in Tables 7 and 8 below), in dB

$G_{csc^2}(\theta)$: the normalized power directivity pattern associated with the cosecant-squared part of the pattern (defined in Tables 7 and 8 below), in dB

G_0: the normalized floor directivity level, in dB

θ_{Start}: elevation (or depression) of the half-power point on the main lobe where cosecant-squared pattern starts (see details below), in degrees

θ_{Null}: one-half $\frac{\sin(x)}{x}$antenna Null-to-Null beamwidth given by $\frac{\theta_3}{0.88}$, in degrees. Using the antenna beam pointing angle, the value for θ_{Null} is $\theta_{Tilt} - \frac{\theta_3}{0.88}$ in degrees for ground radar and $\theta_{Tilt} + \frac{\theta_3}{0.88}$ for airborne radar. This defines the lowest value of the uniform field pattern at the lowest level of the front-to-back ratio

θ_{End}: maximum angle where cosecant-squared pattern stops

θ: angle to evaluate the antenna pattern, in degrees

θ_3: half power antenna beamwidth, in degrees

θ_{Tilt}: antenna beam tilt elevation angle or beam pointing angle, in degrees.

If the operational maximum range and height values, in km, for a radar system application are provided, then the angle where the CSC^2 starts is given by[1]:

$$\theta_{start} = \sin^{-1}\left[\frac{Maximum\_Height}{Maximum\_Range} - \frac{Maximum\_Range}{2*\left(\frac{4}{3}\right)Re}\right] \quad (24)$$

where R_e is the Earth radius of 6 378 km. However, if the operational parameters are not provided then the CSC^2 start angle θ_{Start} is given by the following equations:

$\theta_{Start} = \frac{\theta_3}{2} + \theta_{Tilt}$ for ground radar and $\theta_{Start} = \frac{-\theta_3}{2} + \theta_{Tilt}$ for airborne radar.

The cosecant pattern is applied as shown in Tables 7 and 8.

---

[1] See Barton, David K., *Radar Equations for Modern Radar*, Chapter 2, Artech House Radar Library, 2013.

TABLE 7

Cosecant-squared antenna pattern normalized equations for ground radars

Cosecant-squared equation	Comment	Equation No.
Cosecant floor level G_0 (example = −55 dB)	At angles less than θ_{Null} or more that θ_{End} use −55 dB front to back ratio Note that θ_{Null} is $\theta_{Tilt} - \frac{\theta_3}{0.88}$	(25)
$G_{unif}(\theta) = 20.\log_{10}\left(\frac{\sin(\mu)}{\mu}\right)$ $\mu = (\pi \cdot 50.8 \cdot \sin(\theta - \theta_{Tilt}))/\theta_3$	Use $\frac{\sin(x)}{x}$ from the lower one half the null to-null beamwidth to the start of the CSC^2 pattern at θ_3 *or* θ_{start} whichever is provided	(26)
$G_{csc^2}(\theta)$ $= 20.\log_{10}\left(\frac{CSC(\theta)}{CSC(\theta_{Start})}\right)$ $+ 20.\log_{10}\left(\frac{\sin\left(\frac{\pi \cdot 50.8 \cdot \sin(\theta_{Start} - \theta_{tilt})}{\theta_3}\right)}{\frac{\pi \cdot 50.8 \cdot \sin(\theta_{Start} - \theta\_tilt)}{\theta_3}}\right)$ ◦	Start the CSC^2 pattern up to the maximum CSC^2 angle The gain at θ_{Start} is the gain of the $\frac{sin(x)}{x}$pattern at θ_{Start}. The pattern gain is lower than the peak antenna gain by 3 dB at θ_{Start}	(27)

TABLE 8

Cosecant-squared antenna pattern normalized equations for airborne radars

Cosecant-squared equation	Comment	Equation No.
Cosecant floor level G_0 (example = −55)	At angles less than θ_{Null} or more that θ_{End} use −55 dB front to back ratio. Note that θ_{Null} is $\theta_{Tilt} + \frac{\theta_3}{0.88}$	(28)
$G_{unif}(\theta) = 20.\log_{10}\left(\frac{\sin(\mu)}{\mu}\right)$ $\mu = (\pi \cdot 50.8 \cdot \sin(\theta - \theta_{Tilt}))/\theta_3$	Use $\frac{\sin(x)}{x}$ from the lower one half the null to-null beamwidth to the start of the CSC^2 pattern at θ_3 or θ_{start} whichever is provided	(29)
$G_{csc^2}(\theta)$ $= 20.\log_{10}\left(\frac{CSC(\theta)}{CSC(\theta_{Start})}\right)$ $+ 20.\log_{10}\left(\frac{\sin\left(\frac{\pi \cdot 50.8 \cdot \sin(\theta_{Start} - \theta_{tilt})}{\theta_3}\right)}{\frac{\pi \cdot 50.8 \cdot \sin(\theta_{Start} - \theta_{tilt})}{\theta_3}}\right)$ ◦	Start the CSC^2 pattern up to the maximum CSC^2 angle The gain at θ_{Start} is the gain of the $\frac{\sin(x)}{x}$pattern at θ_{Start}. The pattern gain is lower than the peak antenna gain by 3 dB at θ_{Start}	(30)

A graphical description of the patterns is shown in the Figures below.

FIGURE 7

Cosecant squared beam coverage for search radar

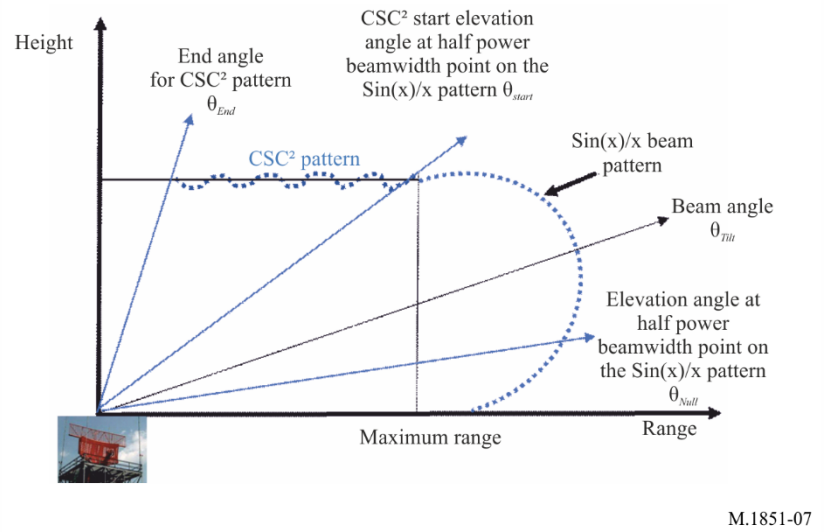

FIGURE 8

Cosecant squared beam coverage for airborne radar

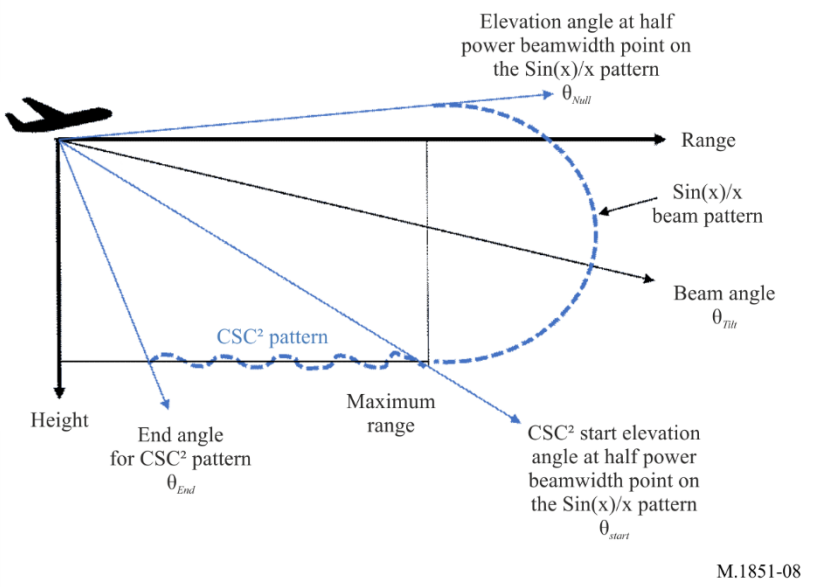

An example using the above procedure provides an antenna pattern for radar C parameters (from Recommendation ITU-R M.1462-2; the Figure itself does not appear in M.1462-2) and is shown below.

FIGURE 9

Example of ground radar – Cosecant squared theoretical antenna directivity.
Gain = 33.5 dBi, $\theta_{3dB} = 4.8°$, $\theta_{Start} = 4.4°$, $\theta_{End} = 30.0°$, $\theta_{Null} = -3.5°$, $\theta_{Tilt} = 2.0°$

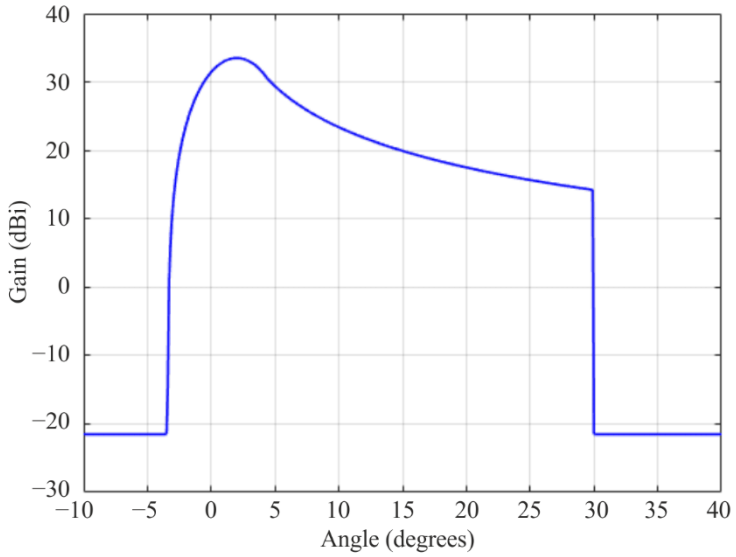

M.1851-09

For airborne radar the inverted CSC^2, elevation antenna pattern is shown below.

FIGURE 10

Example of aircraft radar – Cosecant squared theoretical antenna directivity.
Gain = 33.5 dBi, $\theta_{3dB} = 4.8°$, $\theta_{Start} = -7.4°$, $\theta_{End} = -30.0°$, $\theta_{Null} = 0.5°$, $\theta_{Tilt} = -5.0°$

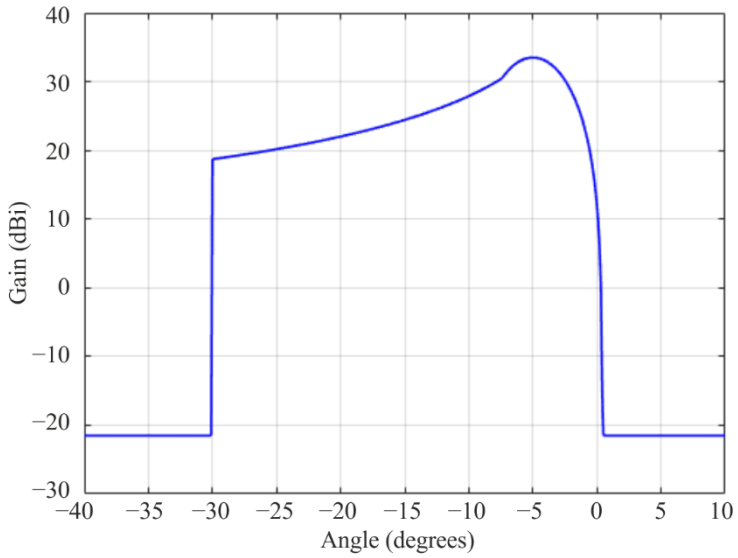

M.1851-10

2.3 Theoretical diagrams and masks for different antenna radiation patterns

FIGURE 11

Antenna normalised, peak, and average envelope for uniform field distribution

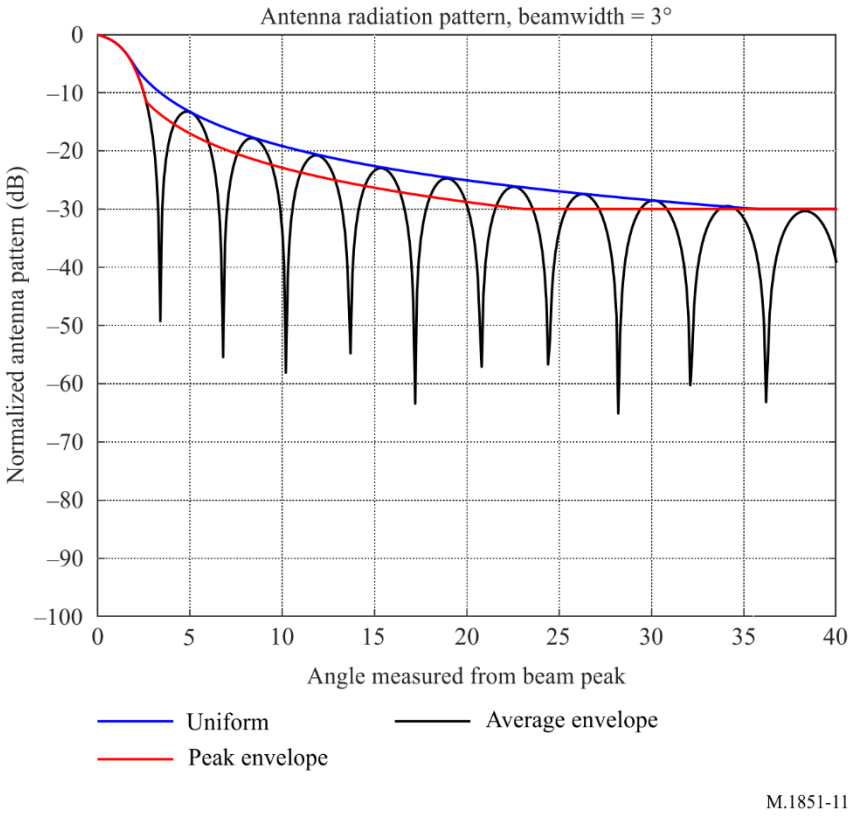

FIGURE 12

Normalised example polar plot antenna pattern, peak degrees, and average envelope for uniform field distribution

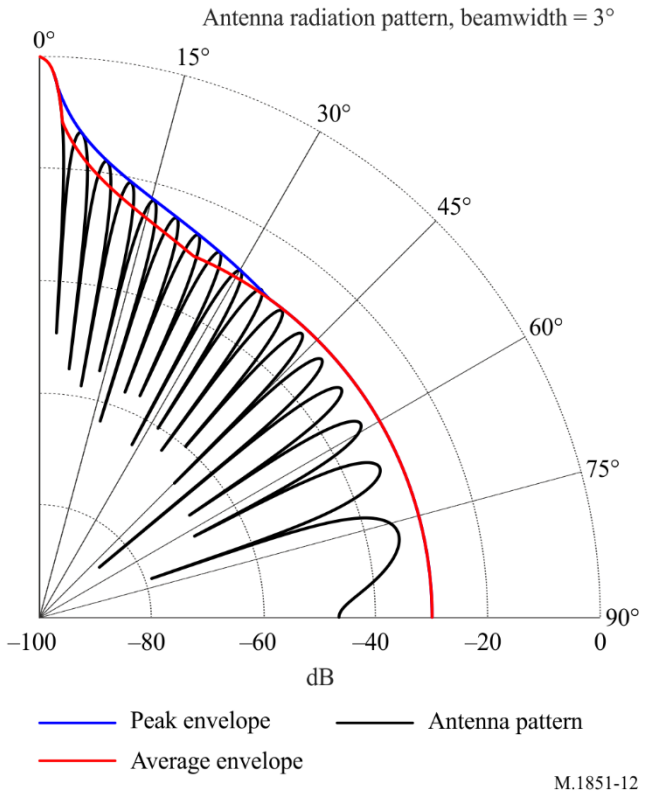

FIGURE 13

Antenna pattern, peak and average envelope for cosine field distribution

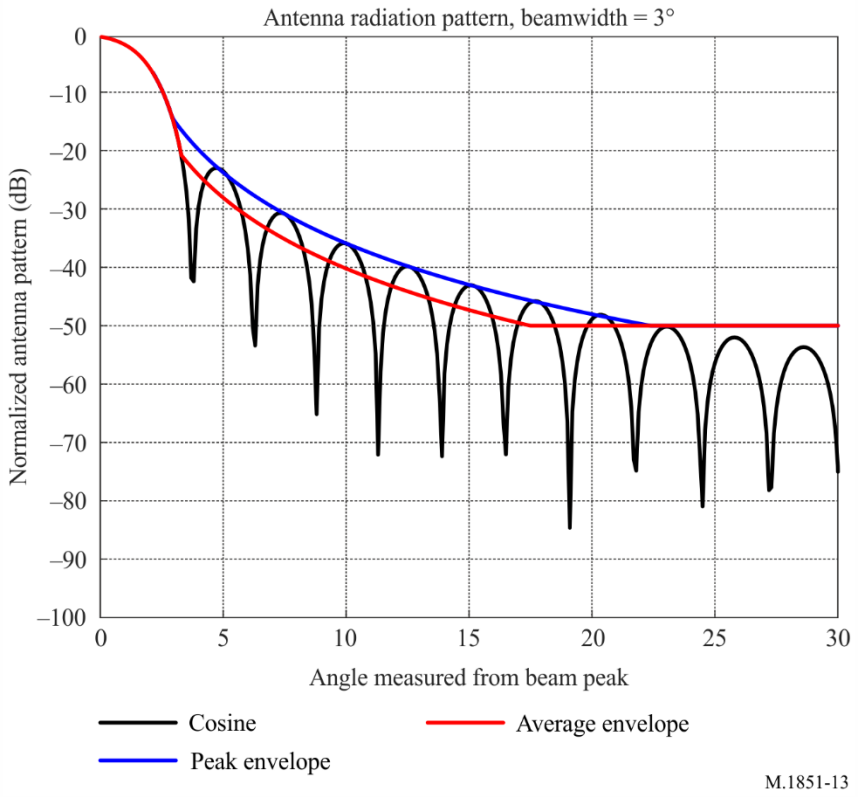

FIGURE 14

Antenna normalised pattern, degrees, peak and average envelope for a cosine-squared distribution

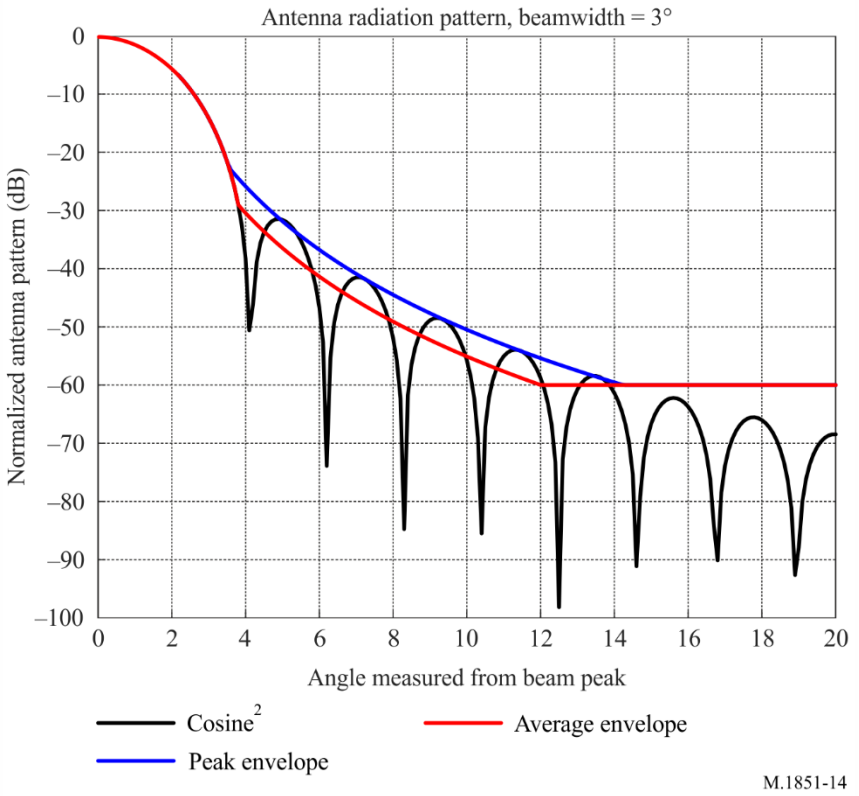

FIGURE 15

Antenna normalised pattern, degrees peak and average envelope for a cosine-cube distribution

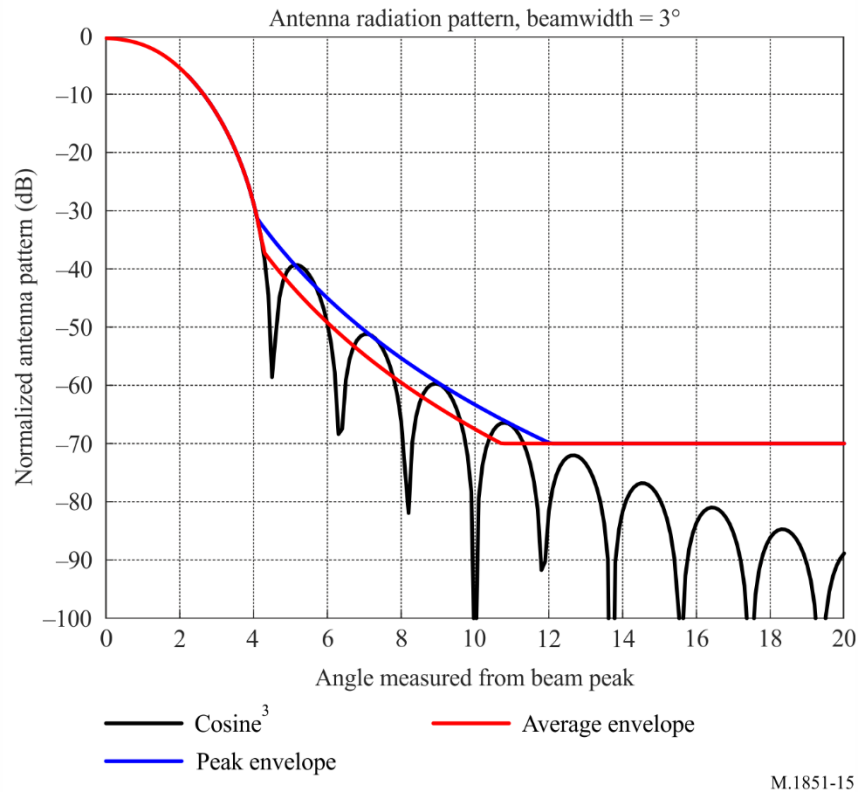

FIGURE 16

Antenna normalised pattern, degrees, peak and average envelope for a cosine-to-the-fourth power distribution

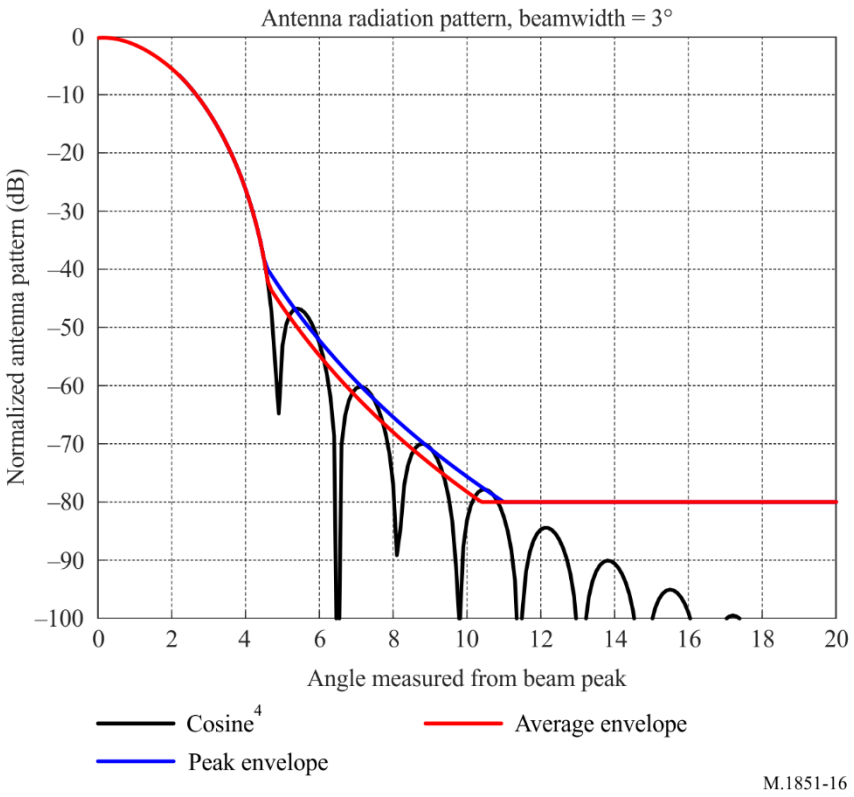

2.4 Antenna pattern selection for models without pedestals

A suggestion for how the antenna pattern should be selected is based on information about half-power beamwidth and peak side-lobe level. This is provided in Table 9 given information about half power beamwidth. This model gives discrete values of sidelobe levels −13.2 dB, −23 dB, −32 dB, −40 dB and −47 dB.

TABLE 9

Pattern approximation selection table

Range of first side-lobe level below normalized main lobe peak (dB)	Possible antenna distribution type and cosine raised to power *n*	Theoretical pattern equation number	Mask equation number
13.2 to < 20	Uniform	(2)	(7)
20 to < 30	$n = 1$	(3)	(8)
30 to < 39	$n = 2$	(4)	(9)
39 to < 45	$n = 3$	(5)	(10)
≥ 45	$n = 4$	(6)	(11)

3 Antenna pattern comparison

One mathematical model for a radiodetermination radar antenna pattern that has been used in interference analysis is given in Recommendation ITU-R M.1652. It includes equations for several patterns as a function of antenna gain. A comparison between the models developed in this Recommendation and Radar-C from Recommendation ITU-R M.1638-0 shows that the pattern in Recommendation ITU-R M.1652 is not optimal. As shown in Fig. 17, the pattern from Recommendation ITU-R M.1652 significantly overestimates the antenna gain off the antenna boresight (0°).

It should also be noted that the equations defined in Recommendation ITU-R F.699 tends to overestimate the sidelobe levels of some radar systems, and it was not developed for radar systems.

FIGURE 17

Antenna pattern comparison

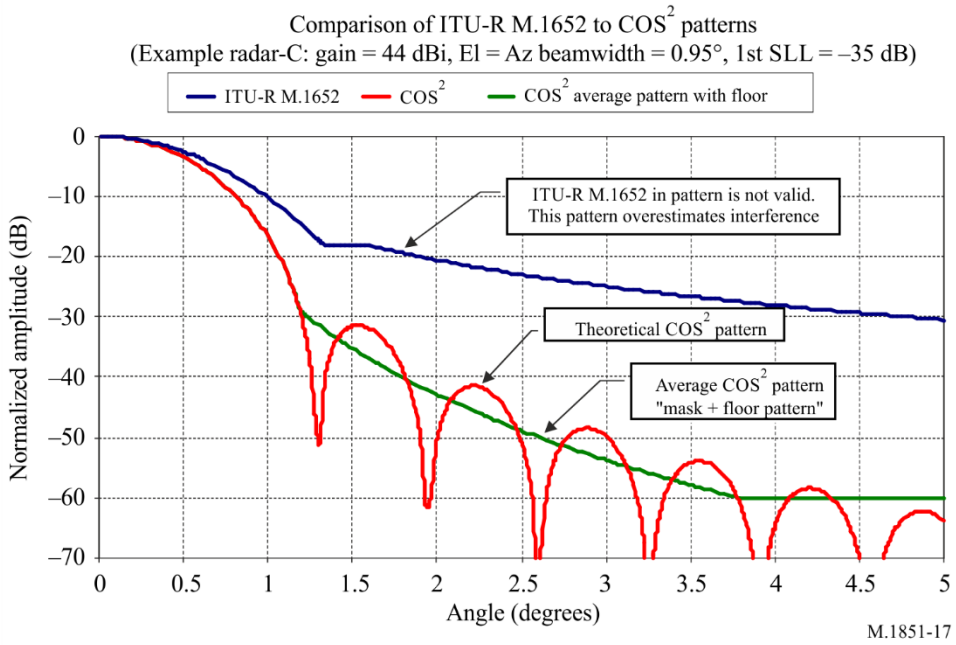

4 Circular parabolic taper aperture antenna

This section describes parabolic taper aperture antenna radiation pattern as well as peak and average envelope radiation patterns for use in interference analyses. When information on the antenna half-power beamwidth and peak sidelobe level are provided, the proper set of equations for peak and average patterns may be selected. Peak sidelobe envelope patterns are used for a single entry interferer and average sidelobe envelope patterns are used for multiple interferers.

4.1 Parabolic antenna use and pattern description

A parabolic antenna is an antenna that uses a parabolic reflector, a curved surface with the cross-sectional shape of a parabola, to direct the radio waves. The most common reflector antennas are the corner reflector antenna, parabolic antenna, paraboloidal antenna, and Cassegrain antenna. Parabolic antennas can have some of the highest gains and narrowest beamwidths of any antenna type. To achieve narrow beamwidths, the parabolic reflector diameter must be much larger than the wavelength of the radio waves used.

Parabolic antennas are used for tracking-radars (like ships, airplanes and clouds), point-to-point communications, wireless links for data communications, satellite communications and spacecraft

communication antennas. They are also used in radio telescopes. The ITU-R has many Recommendations for these applications, such as ITU-R F.699, specifying in *recommends* 4 that where only the beamwidths θ of the antenna are known:

D/λ (expressed in the same unit) may be estimated approximately by the following expression: $\frac{D}{\lambda} \approx \frac{70}{\theta}$ where θ is the beamwidth (−3 dB) (degrees);

given θ, G_{max} may be estimated approximately by: $G_{\max}\ (\text{dBi}) \approx 44.5 - 20 \log \theta$.

The focus here is on the use of parabolic antennas in radar applications, in which there is a need to transmit a narrow beam of radio waves to locate and track objects. For interference analysis there is a need to develop a peak and average antenna sidelobe pattern envelops that only depend on the known antenna half-power beamwidth and peak sidelobe level. The approach used is similar to that of the linear aperture.

From references [1] and [3], the normalized directivity pattern function for parabolic distribution $F(\theta, n)$ for different tapers on a pedestal C is given by the following equation:

$$F(\theta, n) = \frac{\frac{2J_1(\beta a \sin(\theta))}{\beta a \sin(\theta)} + \frac{(1-C)2^{n+1}(n+1)!J_{n+1}(\beta a \sin(\theta))}{n+1 \quad (\beta a \sin(\theta))^{n+1}}}{C + \frac{(1-C)}{n+1}} \tag{31}$$

for models without pedestal:

$$F(\theta, n) = \frac{2^{n+1}(n+1)!J_{n+1}(\beta a \sin(\theta))}{(\beta a \sin(\theta))^{n+1}} \tag{32}$$

where:

β : free space constant = $\frac{2\pi}{\lambda}$, where λ in metre

a : radius of the antenna, in metre

D : antenna diameter, in metre

θ_3 : antenna pattern 3 dB half power beamwidth, in degrees

J_n : Bessel function (can be evaluated with various software tools)

λ : wavelength

n : numeric parabolic taper power value.

In equations (31) and (32), $\beta a = \frac{\pi K}{\theta_3}$ for mathematical model based antenna $\theta_3 = D/\lambda$ (in radians). For model with pedestal, the values for *K* in degrees are provided in Table 10 where $K = \frac{2a\ \theta_3}{\lambda}$ and *SLL* denotes the first sidelobe level, in dB. Equation (31) can be written as:

$$F(\theta, n) = \frac{\frac{2J_1\left(\frac{\pi K}{\theta_3}\sin(\theta)\right)}{\frac{\pi K}{\theta_3}\sin(\theta)} + \frac{(1-C)2^{n+1}(n+1)!J_{n+1}\left(\frac{\pi K}{\theta_3}\sin(\theta)\right)}{n+1 \quad \left(\frac{\pi K}{\theta_3}\sin(\theta)\right)^{n+1}}}{C + \frac{(1-C)}{n+1}} \tag{33}$$

and for models without pedestal, equation (32) can be written as:

$$F(\theta, n) = \frac{2^{n+1}(n+1)!J_{n+1}(\pi K/\theta_3 \sin(\theta))}{(\pi K/\theta_3 \sin(\theta))^{n+1}} \tag{34}$$

The three-dimensional (3D) pattern may be obtained by rotating radiation pattern from equations (33) and (34) around the perpendicular to the aperture.

In Table 10 the relationship between sidelobe level, pedestal C and beamwidth factor is shown. The model with pedestal can give any sidelobe level in the range from −17.66 dB to −44.72 dB. The

ranges of sidelobe levels for each amplitude distributions (n = 0, 1, 2 or 3) are shown in the column 'Range of maximum side-lobe level below normalized main lobe peak (dB)' of Table 10.

The parameters for the model without pedestal are given in Table 11. This model gives discrete values of sidelobe levels −17.66 dB, −24.64 dB, −30.61 dB, −35.96 dB and −40 dB. Also it gives much steeper descending envelope of the sidelobes comparing with the model based on equation (33).

TABLE 10

Table for selection of antenna parameters for circular aperture antenna with pedestal

Parabolic distribution raised to power n	**Range of maximum side-lobe level below normalized main lobe peak (dB)**	**Pedestal C**	**Beamwidth factor K (°)**
0	−17.66	-	58.2125
1	−24.2 to −17.66	$C = 0.0016(SLL + 24.265)^3 - 0.009(SLL + 24.265)^2 + 0.12(SLL + 24.265) + 0.1$ (35)	$K = 0.0051(SLL + 24.265)^4 - 0.089(SLL + 24.265)^3 + 0.599(SLL + 24.265)^2 - 3.11(SLL + 24.265) + 69.43$ (36)
2	−24.2 to −34.7	$C = (0.0022(SLL + 34.7)^3 - 0.032(SLL + 34.7)^2 + 0.38(SLL + 34.7) + 1.1)/10$ (37)	$K = 0.0019(SLL + 34.7)^4 - 0.052(SLL + 34.7)^3 + 0.492(SLL + 34.7)^2 - 2.63(SLL + 34.7) + 74.9$ (38)
3	−44.72 to −34.7	$C = 0.01008\ \mathrm{SLL} + 0.4959$ (39)	$K = 0.0057\ \mathrm{SLL}^3 + 0.7079\ \mathrm{SLL}^2 + 28.061\ \mathrm{SLL} + 433.7618$ (40)

TABLE 11

Table for selection of antenna parameters for circular aperture antenna without pedestal

Parabolic power, n	**Peak sidelobe level (dB)**	**Beamwidth factor K (°)**
0	−17.66	58.2125
1	−24.64	72.5938
2	−30.61	84.0529
3	−35.96	96.3142
4	−40.0	108.2317

4.2 Procedure to compute sidelobe envelope

Using equation (33) and Table 12 for models with pedestal or equation (34) and Table 13 for models without pedestal, it is possible to develop the mask equations. These masks are derived using curve fits to the antenna peak sidelobe levels beyond the antenna pattern first null location. It has been

found, by comparing the integral of the theoretical and the proposed mask patterns, that the difference between the peak and average envelopes in one principal plane cut is 4 dB. The following procedure is used for calculating the peak and average envelops:

1 compute equation (33) for models with pedestal or (34) for models without pedestal for different *n* values using the value of *K* from Table 10 or 11, then normalize the pattern and convert to dB using $20 \times \log_{10}(|\text{Normalized Pattern}|)$;

2 to plot the mask, use the theoretical directivity pattern from equation (33) for models using pedestal or (34) for models without pedestal up to the break point for either the peak or average antenna pattern, as required. After the break point, apply the mask pattern as indicated in Table 12 for models with pedestal or 13 for models without pedestal;

3 the peak pattern mask is the antenna pattern that rides over the sidelobe peaks. It is used for a single-entry interferer;

4 the average pattern mask is the antenna pattern that approximates the integral value of the theoretical pattern. It is used for aggregated interferers;

5 the average pattern mask break point is the point in pattern magnitude (dB) below the maximum gain, where the pattern shape departs from the theoretical pattern into the average mask pattern;

6 the peak pattern mask break point is the point in pattern magnitude (dB) below the maximum gain, where the pattern shape departs from the theoretical pattern into the peak mask pattern;

7 θ_3 is the 3 dB antenna beamwidth (degrees);

8 θ is the angle in either the elevation (vertical) or azimuth (horizontal) principal plane cuts (degrees); and

9 the average mask is computed using the peak mask and subtracting 4 dB. Note that the break points of the peak pattern are different from the average patterns.

10 the three-dimensional (3D) pattern may be obtained by rotating envelope radiation pattern from Table 12 for models with pedestal or Table 13 for models without pedestal around the perpendicular to the aperture.

Tables 12 and 13 show the equations to be used in the calculations of the average and peak antenna masks.

TABLE 12

Equation (41): Peak and average normalised theoretical mask pattern equations for parabolic taper with pedestal

Parabolic distribution raised to power *n*	**Mask equation beyond pattern break point where mask departs from theoretical pattern (dB)**	**A**	**B**	**Mask floor level (dB)**
0	$-A \ln \frac{B\lvert\theta\rvert}{\theta_3}$	12.55	2.394	−35
1		$\mathrm{A} = -0.00227(\mathrm{SLL} + 17.66)^5 - 0.02745(\mathrm{SLL} + 17.66)^4 - 0.1224(\mathrm{SLL} + 17.66)^3 - 0.204(\mathrm{SLL} + 17.66)^2 - 0.1727(\mathrm{SLL} + 17.66) + 12.2586$	if $SLL \geq -24.2$ and $SLL \leq -21.55$: $\mathrm{B} = 0.083177\ \mathrm{SLL}^3 + 5.4731\ \mathrm{SLL}^2 + 119.8649\ \mathrm{SLL} + 877.4646$ if $SLL \geq -21.55$ and $SLL \leq -17.66$: $B = -0.2471\ \mathrm{SLL} - 1.6534$	−50
2		if $SLL \geq -34.7$ and $SLL \leq -31.55$: $\mathrm{A} = -0.06419753\ \mathrm{SLL}^3 - 6.17611\ \mathrm{SLL}^2 - 198.013\ \mathrm{SLL} - 2105.5$ if $SLL \geq -31.55$ and $SLL \leq -24.2$: $A = 0.0053\ \mathrm{SLL}^2 + 0.4366\ \mathrm{SLL} + 18.714$	if $SLL \geq -34.7$ and $SLL \leq -32.6$: $\mathrm{B} = -1.5961\ \mathrm{SLL}^2 - 106.45\ \mathrm{SLL} - 1758.7$ if $SLL \geq -32.6$ and $SLL \leq -24.2$: $\mathrm{B} = 0.0656\ \mathrm{SLL}^2 + 2.574\ \mathrm{SLL} + 29.4$	−60
3		$A = 0.0005(SLL + 34.7)^3 + 0.0022(SLL + 34.7)^2 + 0.0324(SLL + 34.7) + 11.7177$	$\mathrm{B} = -0.0219(\mathrm{SLL} + 34.7)^3 - 0.148(\mathrm{SLL} + 34.7)^2 - 0.856(\mathrm{SLL} + 34.7) + 7.64$	−70

TABLE 13

Peak and average normalized theoretical mask pattern equations without pedestal

Field distribution equation (22)	Mask equation beyond pattern break point where mask departs from theoretical pattern (dB)	Peak pattern break point where mask departs from theoretical pattern (dB)	Average pattern break point where mask departs from theoretical pattern (dB)	Mask front-to-back floor level (dB)	Equation No.
$n = 0$	$-28.9 \times \log_{10}\left(\frac{\lvert\theta\rvert}{\theta_3}\right) - 11.9$	$0.8537 \times \theta_3$	$1.051 \times \theta_3$	−35	(42)
$n = 1$	$-49.0 \times \log_{10}\left(\frac{\lvert\theta\rvert}{\theta_3}\right) - 14.4$	$0.9893 \times \theta_3$	$1.161 \times \theta_3$	−50	(43)
$n = 2$	$-69.13 \times \log_{10}\left(\frac{\lvert\theta\rvert}{\theta_3}\right) - 15.46$	$1.13 \times$	$1.273 \times \theta_3$	−60	(44)
$n = 3$	$-89.0 \times \log_{10}\left(\frac{\lvert\theta\rvert}{\theta_3}\right) - 16.12$	$1.2165 \times \theta_3$	$1.339 \times \theta_3$	−70	(45)
$n = 4$	$-108.8 \times \log_{10}\left(\frac{\lvert\theta\rvert}{\theta_3}\right) - 16.27$	$1.2835 \times$	$1.3906 \times$	−80	(46)

The approach is shown in Fig. 18.

FIGURE 18

Break point example

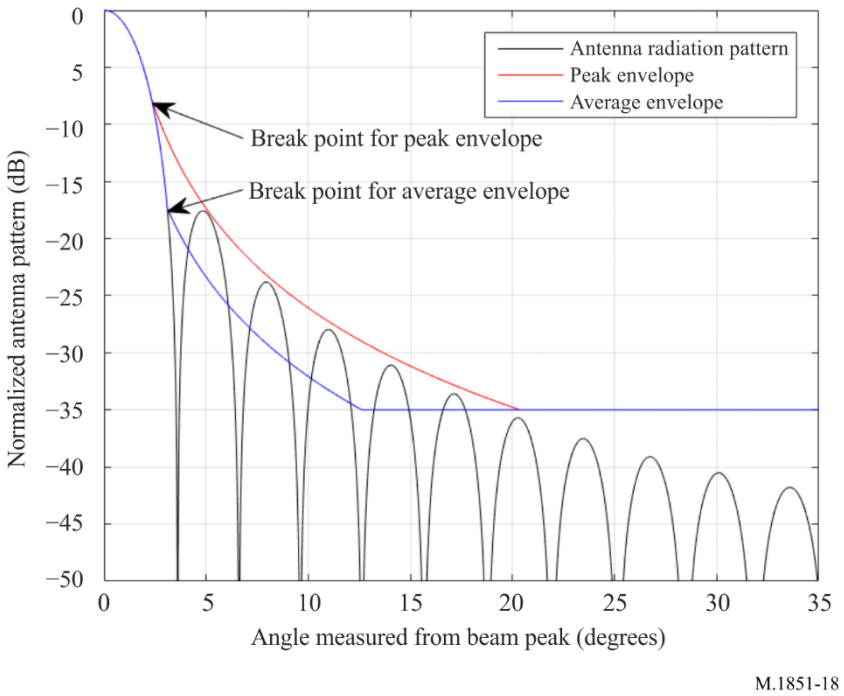

FIGURE 19

Antenna pattern comparison for various circular parabolic taper aperture distributions with pedestal, 3 dB beamwidth is 6.0 degrees (pattern is symmetric)

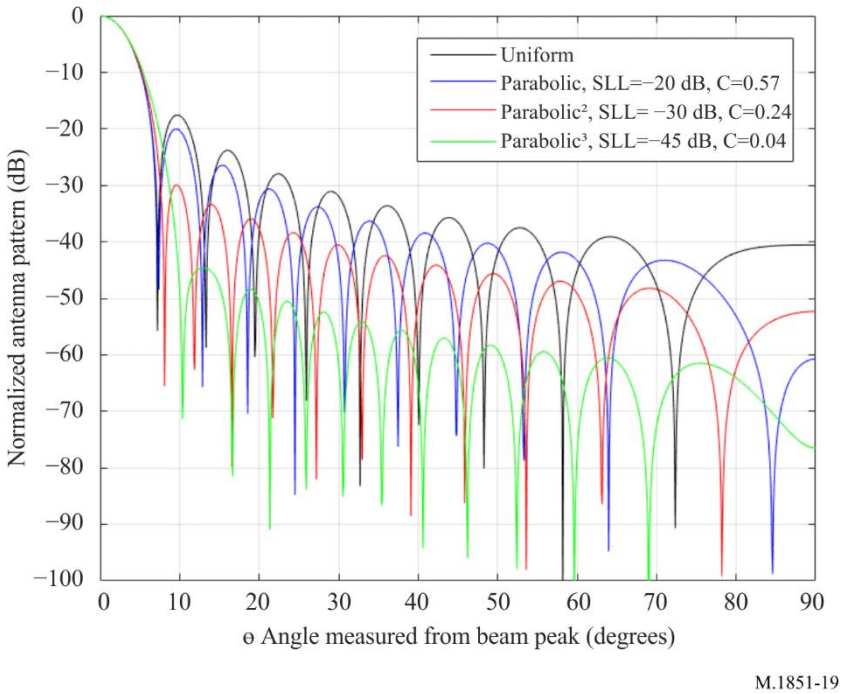

FIGURE 20

Antenna pattern comparison for various circular parabolic taper aperture distributions without pedestal, 3 dB beamwidth is 6.0 degrees (pattern is symmetric)

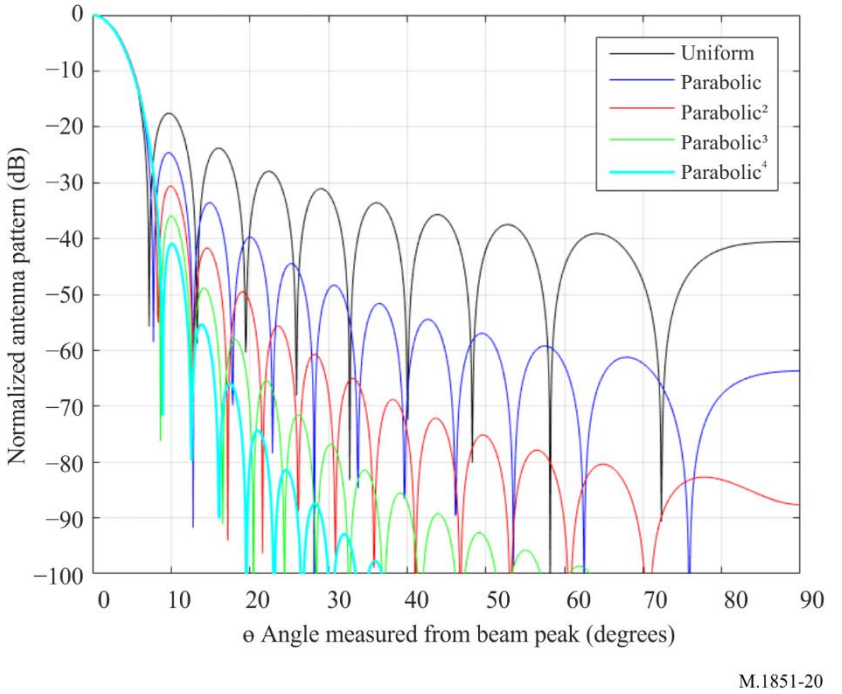

4.3 Antenna pattern selection for models without pedestal

Table 14 provides suggestion for how the antenna pattern should be selected based on information about the peak side-lobe level. This model gives discrete values of sidelobe levels –17.66 dB, –24.64 dB, –30.61 dB, –35.96 dB and –40 dB.

TABLE 14

Parabolic taper as a function of peak sidelobe level

Range of normalized peak side-lobe level (dB)	**Parabolic antenna distribution power,** *n*
–15 to –20	$n = 0$
–20 to –27	$n = 1$
–27 to –33	$n = 2$
–33 to –38	$n = 3$
Less than –38	$n = 4$

References

[1] Barton, David K., and Ward, Harold R., *Handbook of Radar Measurement*, Artech House, 1984, Table A.15, page 264.

[2] Chang, Kai, editor-in-chief, *et al.*, *Encyclopaedia of RF and microwave engineering*, 6 Volume set. Koazkoff, Dennis, *Aperture Antennas*, DeVry University, Alpharetta, Georgia, page 365. The *Encyclopaedia of RF and Microwave Engineering* is available online at http://www.mrw.interscience.wiley.com/erfme

[3] Stutzman, Warren L. and Thiele, Gary A., *Antenna theory and design*, 3rd ed. 2013. Table 9-2, page 389.

5 Approximating three-dimensional (3-D) patterns

In some cases, simulation and prediction techniques require the use of a 3-D antenna radiation pattern. Most antenna manufacturers provide information only about the two principal plane radiation cuts (azimuth/elevation, see coordinate system in Fig. 29) of the antenna used in the simulation. Since the 3-D pattern might be needed, a better estimate of the 3-D radiation using the azimuth and elevation cuts is provided.

In general, the simplest way to approximate the 3-D radiation pattern from its two principal cuts (azimuth and elevation), is by summing the dB values of the available samples for each azimuth and elevation angle. This classic method is widely used in many simulation tools, when 3-D capabilities are required.

In the case of directional antennas, there are several methods that have been defined. See the reference list shows several of these references. Two simple methods have been selected from [3]. These methods are the Summation method and the Weighted Summing Method. These methods are compared to the summing method.

The summing method is defined as adding the available samples of the horizontal and vertical planes in dB. This method is particularly adopted for antennas omnidirectional in azimuth, and may be used when azimuth and elevation principal cuts are available.

$$G_{sum} = G_{az}(\varphi) + G_{el}(\theta)$$

For the weighted summing method in reference [3], the equations used in the reference depend on the horizontal cut G_{az} in dB, defined from −180° to 180°, and the vertical cut G_{el} in dB is defined from −90° to 90°. Only the front elevation gain pattern is used. The elevation backlobe gain pattern is not used in the methodology.

$$G_{az}(\varphi) = 10 \log_{10}(g_{az}(\varphi))$$
$$G_{el}(\theta) = 10 \log_{10}(g_{el}(\theta))$$

At point (θ, φ), the weighted gain GW is approximated by reference [3]:

$$GW(\theta, \varphi) = \frac{G_{az}(\varphi) \times w1 + G_{el}(\theta) \times w2}{\sqrt[k]{w1^k + w2^k}}$$

where $w1$ and $w2$ are given by:

$$w1(\theta, \varphi) = g_{el}(\theta) \times (1 - g_{az}(\varphi))$$
$$w2(\theta, \varphi) = g_{az}(\varphi) \times (1 - g_{el}(\theta))$$

It was stated in [3] that the concept behind this technique is that the estimation process of a radiation sample involves the actual data of the other principal elevation and azimuth pattern, as a function of angular distance between the point of interest and the sample point, in a cross-weighting manner between the two principal cuts.

In this approach, the weighting function provides with the means for appropriate angular distance weighting.

A value of k equal to 2 was found to work appropriately for directional antennas but other approximations may also be considered.

In regards with use of § 2.1 (rectangular aperture antenna) the 3D-pattern radiation patterns or envelope patterns may be obtained by equation (14). In regards with use of § 4 (circular aperture) the 3D-pattern radiation patterns or envelope patterns may be obtained by rotating the 2D-pattern. If measured antenna radiation patterns are available, the same methods may be used depending on the type of the considered antenna.

Figures 21 and 22 show an example of a 3-D pattern from its 2-D plane cuts given in Fig. 23.

FIGURE 21

Example contour normalized (dB) antenna pattern computed from its plane cuts in Fig. 23

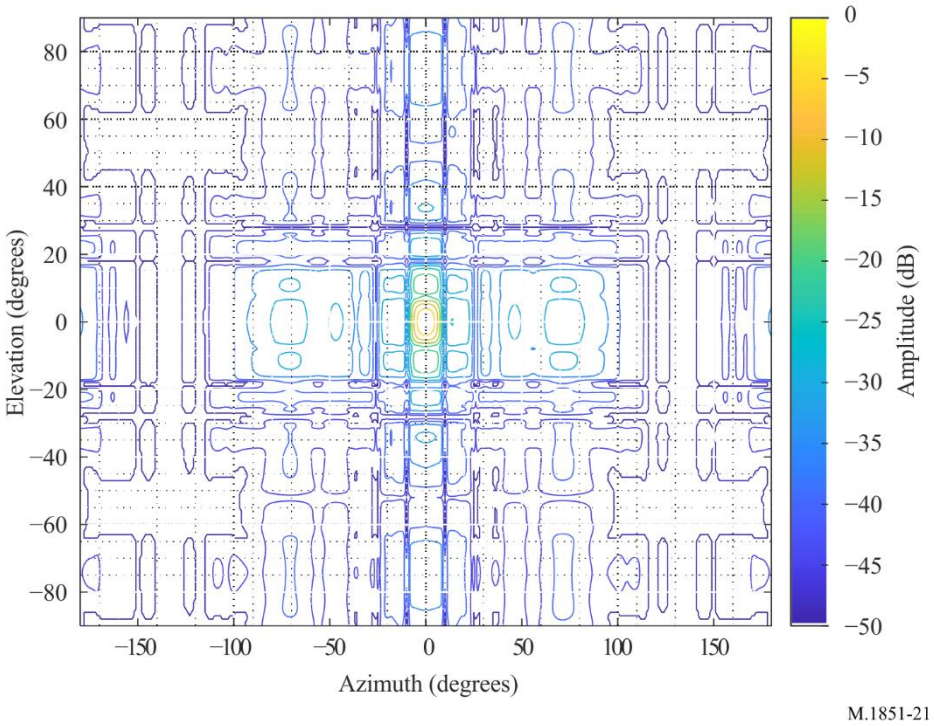

FIGURE 22

Example of a 3-D relative azimuth and elevation antenna plot computed from its plane cuts in Fig. 23

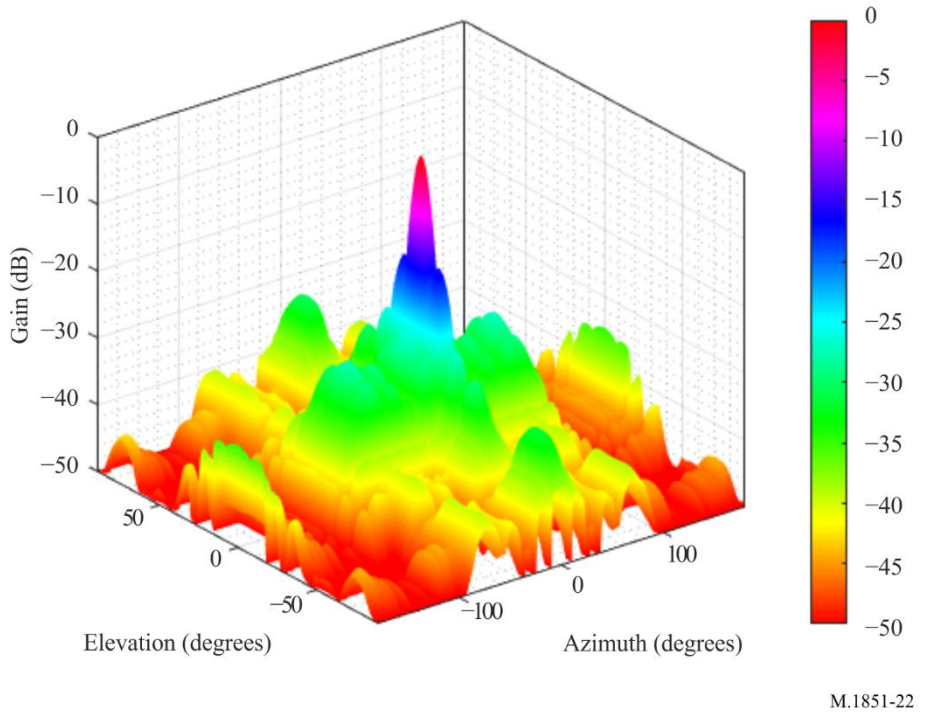

FIGURE 23

Plane cuts of the antenna used as an example to compute 3-D patterns[2]

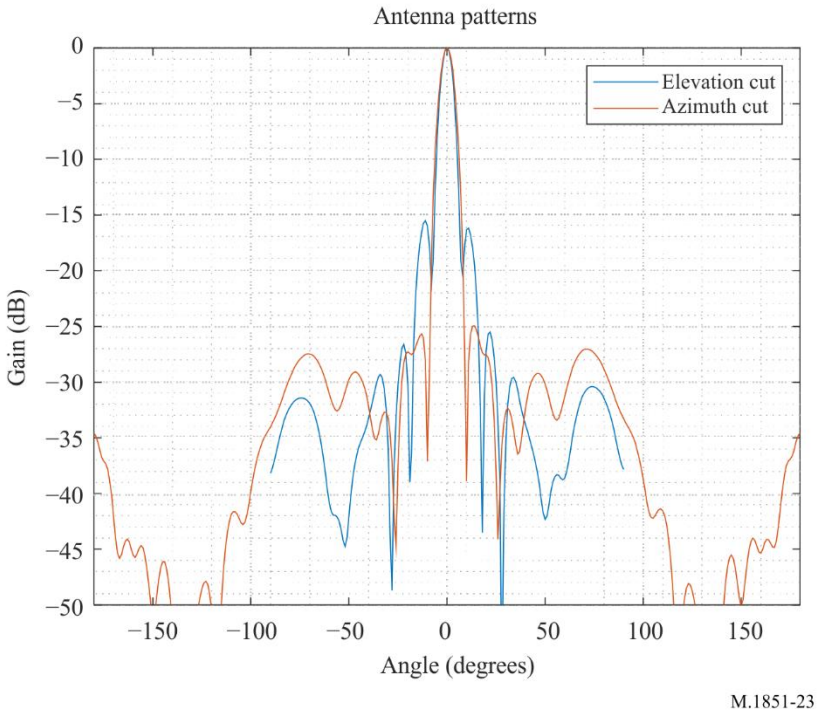

6 Patterns for phased array antennas

6.1 Linear phased antenna array

The following equation could be used in the calculations for uniform linear array antenna normalized pattern:

$$g(\theta) = f(\theta) \cdot \frac{1}{N} |AF(\theta)|^2 \tag{47}$$

where:

g(θ): uniform linear array antenna normalized gain pattern

f(θ): Elementary radiating elements normalized gain pattern inserted in the uniform linear array antenna

N: number of elementary radiating elements

AF(θ): uniform linear array antenna factor:

$$AF(\theta) = \frac{\sin\left(\frac{N\Psi}{2}\right)}{\sin\left(\frac{\Psi}{2}\right)} \tag{48}$$

with

$$\Psi(\theta) = 2\pi(d/\lambda)(\sin(\theta) - \sin(\omega)) \tag{49}$$

where:

d : uniform elementary radiating element regular interspace

[2] Measurements from an RF Elements UltraDishTM TP 27 antenna.

λ : wavelength at the considered frequency

ω : electronically beam steering angle

θ : off-axis angle

N: number of elementary radiating elements.

FIGURE 24

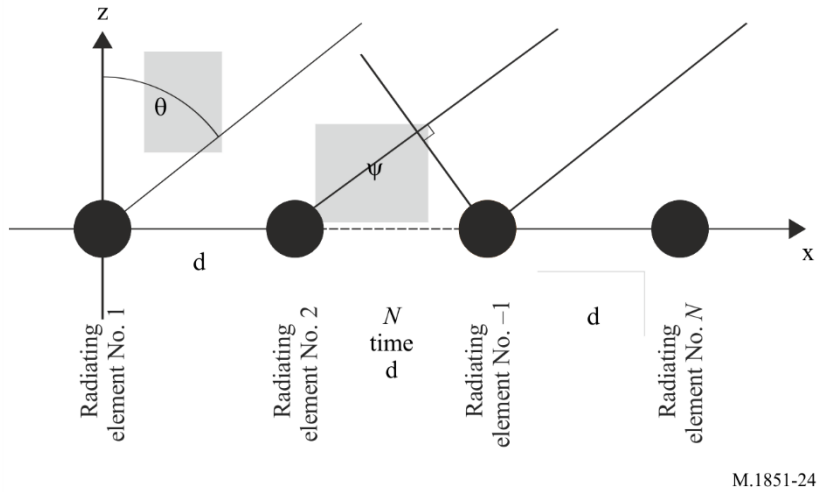

The specific nature of phased array antennas allows to steer electronically the mainlobe of the antenna pattern range from the mechanical antenna boresight. At large scan ω angles specific sidelobes effects in the antenna patterns should be taken into account as mainlobe significant enlargement and de-symmetrisation (see Fig. 25). In fact the main lobe maximum value decreases as cos(ω) and further as the elementary radiating element pattern in the array. This result is a widened mainbeam, max gain losses, and consequently far sidelobes increase. For value of ω between ±60° and ±90° range from the mechanical antenna boresight the resulting pattern is so perturbed that it is no more usable (see Fig. 26). The practical values of ω are between 0° and ±60° range from the mechanical antenna boresight. Furthermore, if the array lattice is bigger than $\lambda/2$ among the elementary radiating elements in the array, grating lobes of the mainlobe could appear for ω even less than ±60° range from the mechanical antenna boresight (see Fig. 27). And even if the array lattice is $\lambda/2$ among the elementary radiating elements in the array, sidelobes of the grating lobes of the mainlobe, situated at −90° and +90° from the mechanical antenna boresight, disturb the array pattern (see Fig. 28) as well as significant mainlobe enlargement and de-symmetrisation.

FIGURE 25

Theoretical normalised radiating pattern of an uniform linear array of 30 radiating elements with a λ/2 lattice (blue curve) steered at boresight with a cosine^2 element radiating pattern (red curve)

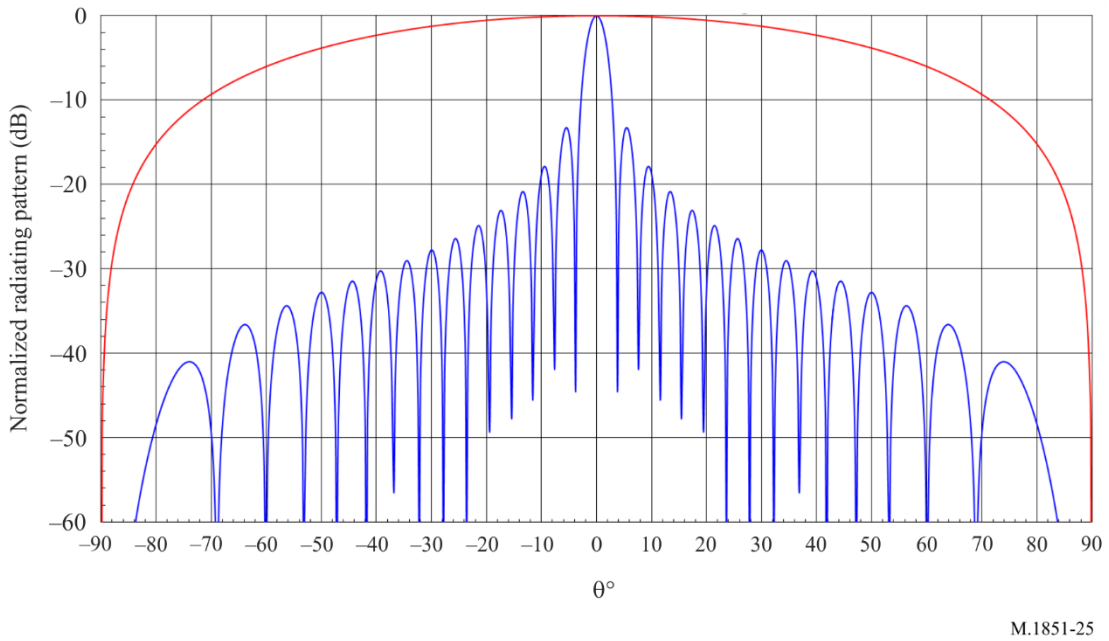

FIGURE 26

Theoretical radiating pattern of a uniform linear array of 30 radiating elements with a λ/2 lattice (blue curve) steered at 60° with a cosine^2 element radiating pattern (red curve)

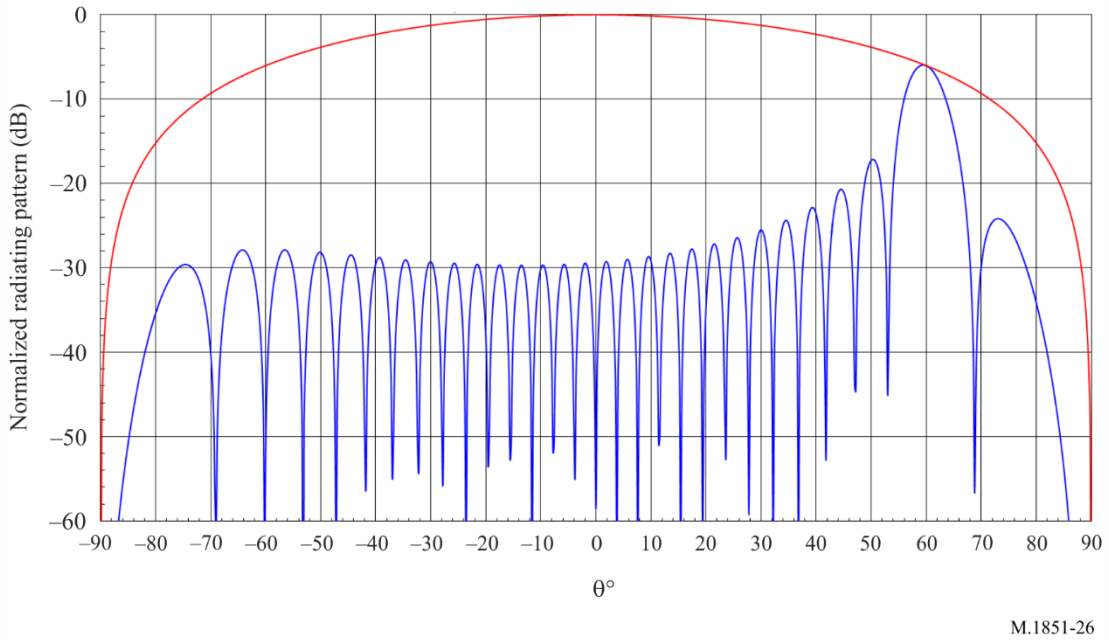

FIGURE 27

Theoretical radiating pattern of a uniform linear array of 30 radiating elements with a 0.6λ lattice (blue curve) steered at 45° with a cosine² element radiating pattern (red curve)

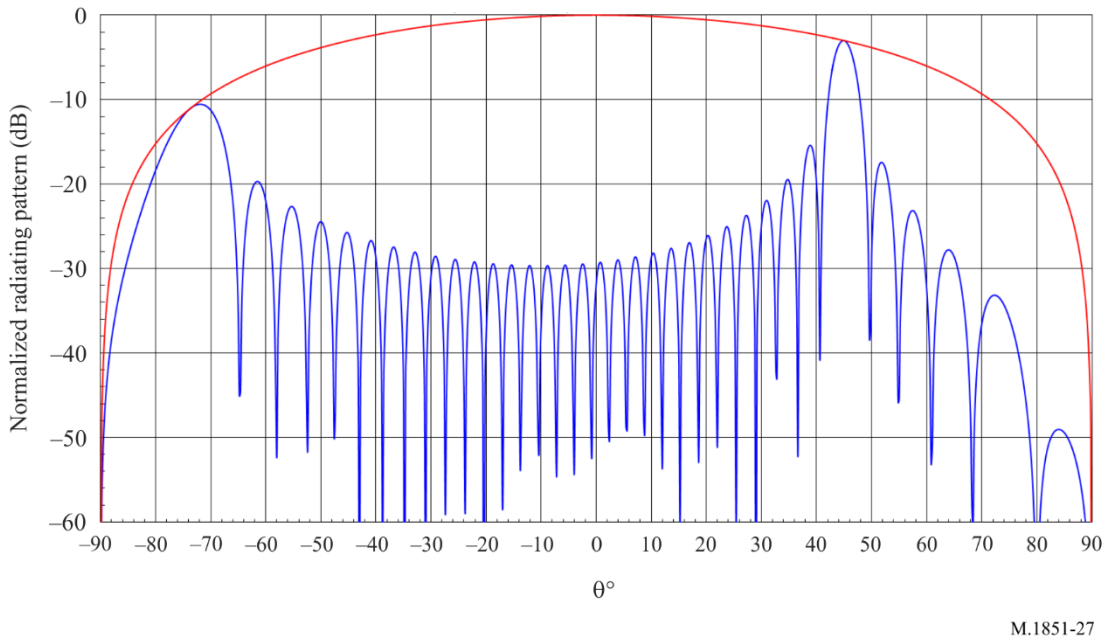

FIGURE 28

Theoretical radiating pattern of a uniform linear array of 30 radiating elements with a λ/2 lattice (blue curve) steered at 80° with a cosine² element radiating pattern (red curve)

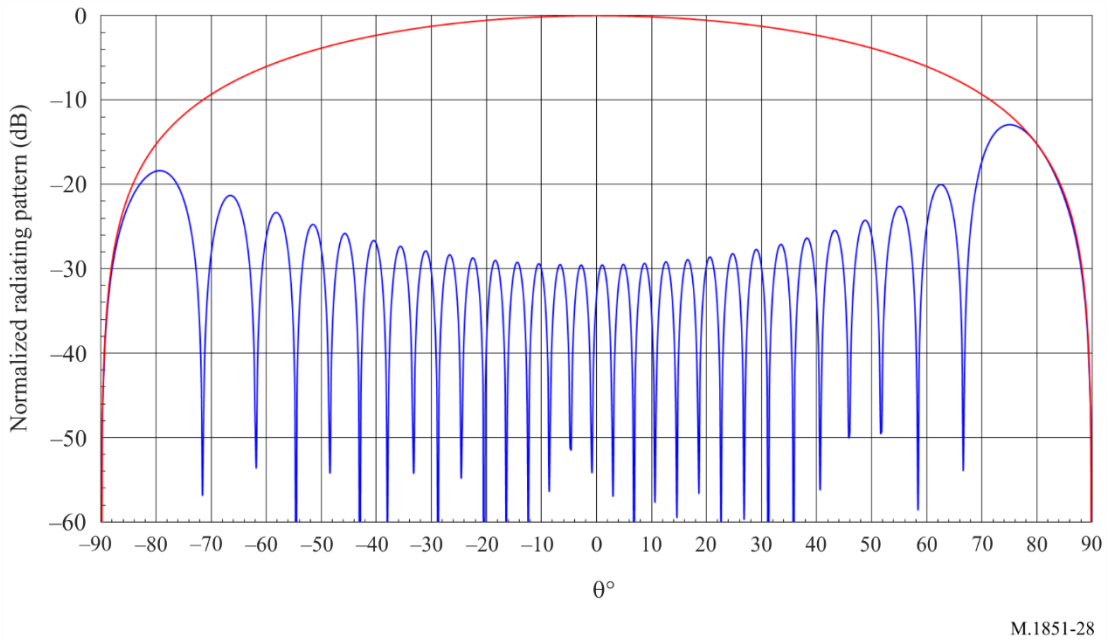

6.2 Planar phased antenna array

Planar arrays are typically a set of identical radiating single elements (e.g. monopoles, dipoles, microstrips…) within a plane. They are generally organized/spaced in a regular structure, resulting in a typical geometry such as rectangular, hexagonal, circular, etc. Planar arrays enable to scan the main beam in any direction of θ (elevation) and φ (azimuth) in any direction of 3-D space.

Thus, the 3D radiation pattern of the planar array can be expressed through two elements:

a) the **single element** directivity $D_e(\theta,\varphi)$ in every angular direction (θ,φ) (either through a pattern or through the physical features such as height, width, length, dielectric constant ε_r of the element, etc.),

b) the **array factor** $AF_{(\theta_{e-tilt},\varphi_{scan})}(\theta,\varphi)$ as a function of the beam steering orientation $(\theta_{e-tilt},\varphi_{scan})$ and angular direction (θ,φ) (through the geometry of the array, the number of elements, the inter-element spacing and through the weighting coefficients at elements of the phased array: uniform or not).

From these two elements, the directivity of the planar array $D_a(\theta,\varphi,\theta_{e-tilt},\varphi_{scan})$ can be expressed as follows:

$$D_a(\theta,\varphi,\theta_{e-tilt},\varphi_{scan}) = 4\pi \frac{D_e(\theta,\varphi).\left|AF_{(\theta_{e-tilt},\varphi_{scan})}(\theta,\varphi)\right|^2}{\int_{-\pi}^{\pi}\int_{0}^{\pi} D_e(\theta',\varphi').\left|AF_{(\theta_{e-tilt},\varphi_{scan})}(\theta',\varphi')\right|^2 \sin\theta' d\theta' d\varphi'}$$

By applying the efficiency factor η of the planar array, the gain pattern $G_a(\theta,\varphi,\theta_{e-tilt},\varphi_{scan})$ of the beam steering orientation $(\theta_{e-tilt},\varphi_{scan})$ and angular direction (θ,φ) can be established:

$$G_a(\theta,\varphi,\theta_{e-tilt},\varphi_{scan}) = \eta.D_a(\theta,\varphi,\theta_{e-tilt},\varphi_{scan})$$

The following equation would capture the directivity for the case of planar antenna array with rectangular lattice as follows:

$$D_a(\theta,\varphi) = D_e(\theta,\varphi).\frac{1}{N}.|AF(\theta,\varphi)|^2 \quad (50)$$

where:

θ: elevation angle (radians)

φ: azimuth angle (radians)

$D_a(\theta,\varphi)$: uniform planar array antenna directivity pattern

$D_e(\theta,\varphi)$: elementary radiating elements directivity pattern inserted in the uniform planar array antenna

N_x: number of elementary radiating elements along the x axis

N_y: number of elementary radiating elements along the y axis

$N = N_x.N_y$: total number of elementary radiating elements

AF: uniform planar array antenna factor:

$$AF(\theta,\varphi) = \frac{\sin\left(\frac{N_x\psi_x(\theta,\varphi)}{2}\right)}{\sin\left(\frac{\psi_x(\theta,\varphi)}{2}\right)} \times \frac{\sin\left(\frac{N_y\psi_y(\theta,\varphi)}{2}\right)}{\sin\left(\frac{\psi_y(\theta,\varphi)}{2}\right)} \quad (51)$$

with

$$\psi_x(\theta,\varphi) = 2\pi \times \frac{d_x}{\lambda} \times \left(\sin(\theta)\times\cos(\varphi) - \sin(\omega_\theta)\times\cos(\omega_\varphi)\right) \quad (52)$$

$$\psi_y(\theta,\varphi) = 2\pi \frac{d_y}{\lambda} \times \left(\sin(\theta)\times\sin(\varphi) - \sin(\omega_\theta)\times\sin(\omega_\varphi)\right) \quad (53)$$

where

d_x: uniform elementary radiating element regular interspace along the x-axis (m)

d_y: uniform elementary radiating element regular interspace along the y-axis (m)

λ: wavelength at the considered frequency (m)

ω_θ: electronical beam elevation steering angle (radians)

ω_φ: electronical beam azimuth steering angle (radians).

FIGURE 29

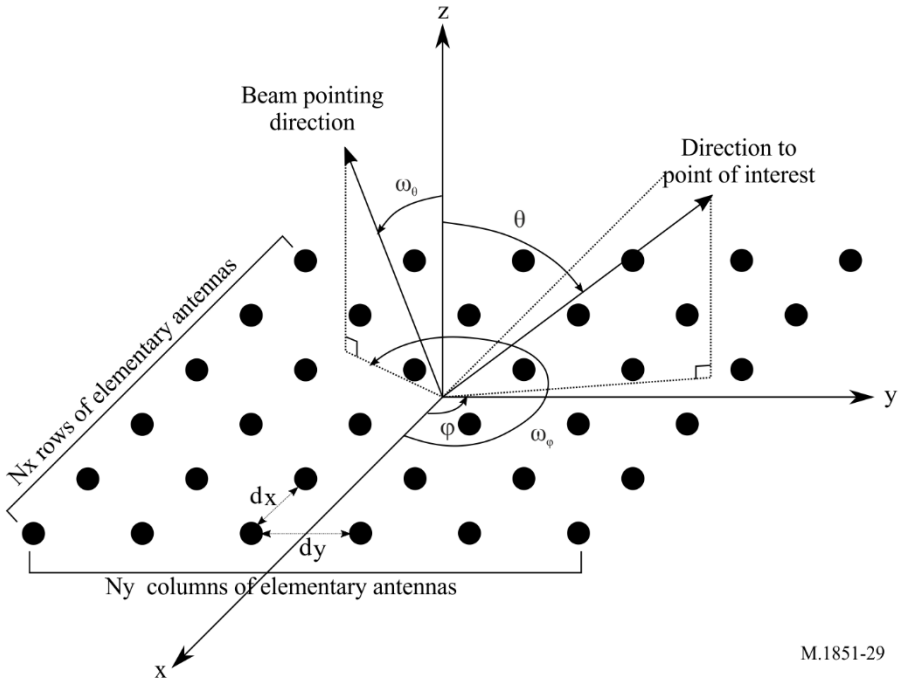

Similar to linear phased array of antennas, planar phased array allows to electronically steer the mainlobe of the antenna towards any spherical coordinates. However, large azimuth and elevation steering angles yields specific sidelφobes effects in the antenna pattern, as well as significant mainlobe enlargement and desymmetrization. The grating lobes are the same as described in § 6.1.

The model of this section requires knowledge of the number of elements (Nx, Ny), element spacing (dx, dy), single element radiation pattern and associated gain of elements. In absence of any knowledge of these input parameters, peak or average masks, as described in § 2.1.1 should be used.

7 Antenna efficiency

Antenna efficiency quantifies the portion of the power supplied to the antenna that actually is radiated, and is defined as the ratio (in linear units of power) between the two quantities and must be strictly lower than 1 (or, equivalently, 0 dB). As a consequence, some care must be taken when using one the model of this Recommendation, in order to ensure that the generated antenna gain pattern complies with this constrain on the antenna efficiency.

Total Integrated Gain (TIG) calculus is possible when the 3D radiation pattern of an antenna is available. TIG may be overestimated for cases where the antenna peak or average masks are used. TIG is defined in linear units as:

$$\mathrm{TIG} = \frac{1}{4\pi}\int_{-\pi}^{\pi}\int_{0}^{\pi} G(\theta,\varphi)\sin(\theta)\,d\theta d\varphi$$

where:

θ: elevation angle (radians)

φ: azimuth angle (radians)

$G(\theta,\varphi)$: antenna gain with respect to an isotropic antenna (linear).

8 Measured pattern examples

Figures 30 and 31 show examples of measured radar antenna patterns, in the 9 GHz band. The X axis represents the azimuth angle spanned on more than 360°, and Y axis represents the power level received at each azimuth angle. The power pattern is normalized to its maximum or to an isotropic antenna to be considered as the normalized antenna pattern or the directivity pattern.

First analysis of such measured antenna patterns indicates that first sidelobes appear near −30 dBc with a noticeable slope of sidelobes leading to estimate roughly that a $\cos^2$ aperture illumination law was used. A theoretical mask floor at −60 dBc given by $\cos^2$ model would appear in this case a bit too low due to presence of backlobe and rear diffraction lobes in this antenna pattern, then if necessary, use real antenna patterns instead of theoretical ones when possible.

Figure 30 shows an example of measured cosecant squared patterns. The radar beams are obtained from a reflector antenna, fed by two horns which deliver two beams tilted at different elevation angles.

FIGURE 30

Example measured antenna plot

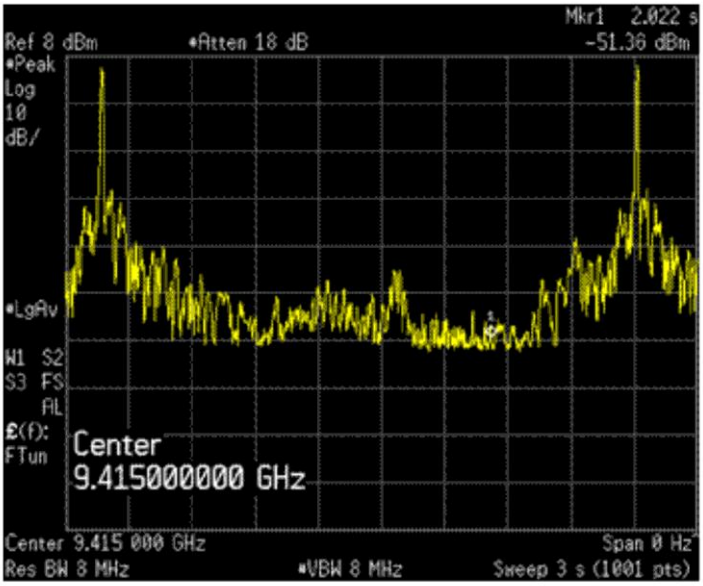

M.1851-30

FIGURE 31

Example measured antenna plot

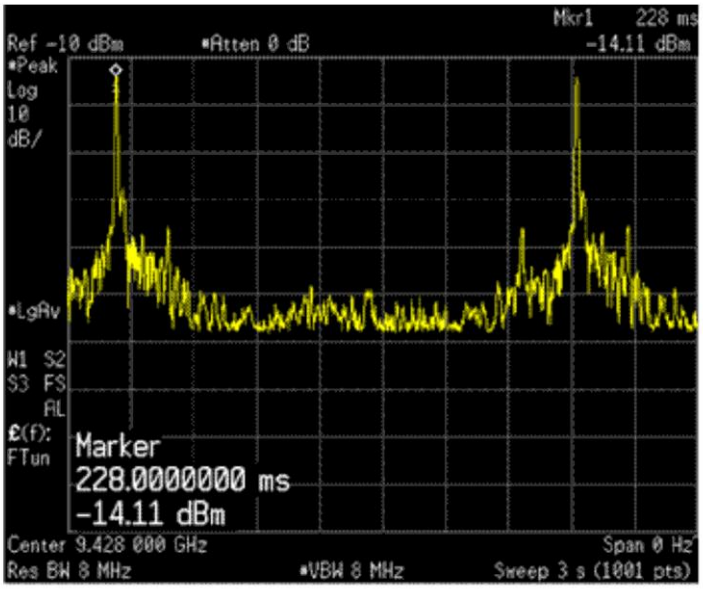

M.1851-31

Figures 32 and 33 show two other examples.

FIGURE 32

Measurement from AN/SPN-6 radar antenna at 3.6 GHz and 38 dBi

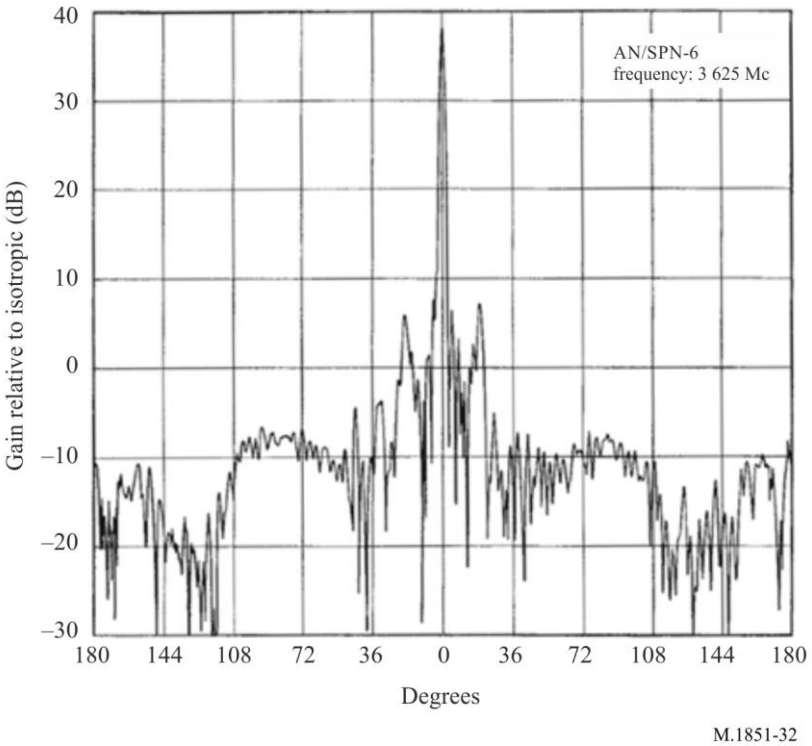

M.1851-32

FIGURE 33

Doppler radar antenna pattern from meteorological radar with 25 dB 1st sidelobe and 60 dB front-to-back ratio

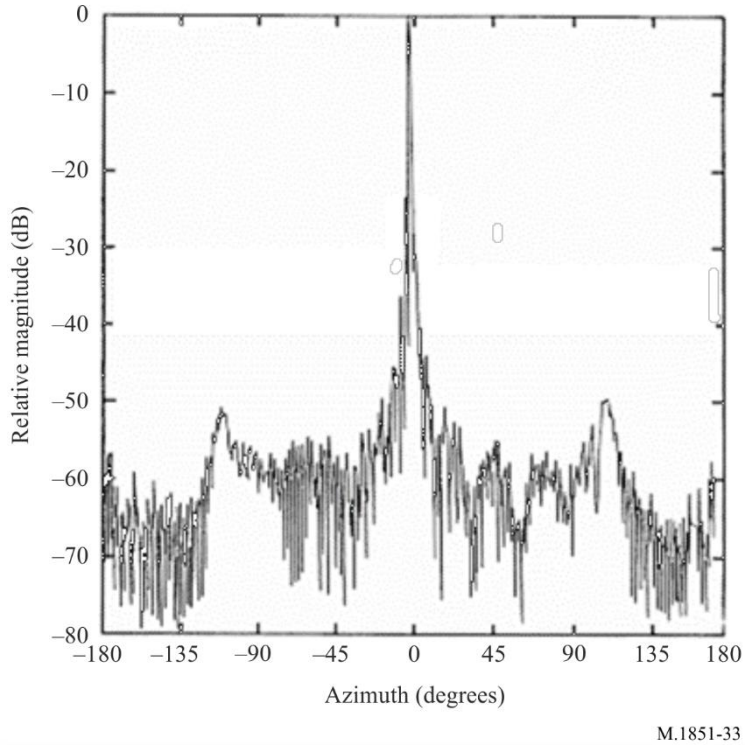

Figure 34 can be compared to the theoretical pattern of cosecant squared antenna given by equations (22) and (23).

FIGURE 34

Measurement from STAR2000 air traffic control (ATC) radar at 2.8 GHz